

https://dspace.org/

Experimental investigation of combined infra-red suppression and tail rotor elimination helicopter anti-torque system

Bouwer, Pieter

2016-08-17
http://hdl.handle.net/10539/20891

Downloaded from a DSpace repository. https://dspace.org/

Experimental investigation of Combined Infra-Red Suppression and Tail rotor Elimination Helicopter Anti-torque system

AUTHOR : Pieter Bouwer
SUPERVISOR : Professor A Nurick

BRANCH OF AERONAUTICAL ENGINEERING
UNIVERSITY OF THE WITWATERSRAND

Abstract

An experimental investigation was carried out on a half scale model of a helicopter Combined Infra-Red Suppression and Tail rotor Elimination (CIRSTEL) system to characterise its performance in terms of power consumption, thrust, pressure drops and temperature reduction. The model consists of a Circulation Control Tail Boom and Thruster (CCTB&T) with the hot engine gasses ducted into the tail boom where they are mixed with ambient air supplied by a fan situated in the body of the helicopter. The CCTB&T replaces the conventional tail rotor on a helicopter and supplies the torque to counter-act the torque applied to the main rotor. The model was tested using both hot and cold air to simulate the flow of hot engine gasses. The performance is defined in terms of thrust, power, and mass flow coefficients which were found to be constant for the configuration tested. It was shown that the power requirements of the fan are significantly reduced by introducing the hot engine gasses into the tail boom. The temperature of the hot engine gasses is also reduced from 450 °C to approximately 200 °C. The surface temperature of the model was found to be less than 55 °C for the configuration.

Acknowledgements

The author wishes to thank the following people:

Professor Alan Nurick for enthusiastic supervision and support, advice and financial assistance.

Jose Martins, Ernst Wilhelm and Johannes Baumbach of the CSIR for technical advice and support during both the design and testing of the model.

Ivan Rademeyer of the CSIR for the use of the HGTF.

Tom Bezuidenhout and Ben Strydom of the CSIR for building the model

Dr Andries Vermeulen and Dr Rob Hurlin of the CSIR for overall support for the programme.

Declaration

I, Pieter Bouwer, declare that this research is my own work. It is being submitted to the Branch of Aeronautical Engineering of the University of the Witwatersrand, Johannesburg, South Africa, for a Degree of Master of Science in Engineering. It has not been submitted before for any other degree

Pieter Bouwer

Nomenclature

A = Area

C = Coefficient

D = Diameter

F = Force

G = Mass flow

K = Coefficient

L = Distance

P = Pressure or Power

Q = Torque

T = Temperature or Thrust

V = Velocity

f = Function

g = Function

q = Dynamic Pressure

ρ = Density

η = Efficiency

λ = Area Ratio

Φ = Flow Ratio

Φ' = Corrected Flow Ratio

θ = Temperature Ratio

Π = Head Pressure Rise

ω = Static Pressure Rise

Subscripts

a = Ambient air from fan

b = Tail boom

d = Diffuser

e = Engine gasses at nozzle exit

f = Final mixture at thruster inlet

p = Power, Pressure

t = Total, Thrust, Thruster

thr = Thruster

Abbreviations

CC	Circulation Control
CCTB	Circulation Control Tail Boom
CCTB&T	Circulation Control Tail Boom and Thruster
CIRSTEL	Combined Infra Red Suppression and Tail rotor ELimination
CSIR	Council for Scientific and Industrial research
DT	Diffuser-Thruster
HGTF	Hot Gas Test Facility

Table of Contents

Abstract i

Acknowledgements ii

Declaration iii

Nomenclature iv

Table of Contents vi

1 Introduction 1
- 1.1 Background 1
- 1.2 Circulation controlled tail boom and thruster 2
- 1.3 Combined infra-red suppression and tail rotor elimination 3
  - 1.3.1 Single flow system 4
  - 1.3.2 Dual flow system 5

2 Objectives 6

3 Literature Survey 7
- 3.1 Jet Thruster 7
  - 3.1.1 CCTB&T 8
    - 3.1.1.1 Thrust 8
    - 3.1.1.2 Power 10
  - 3.1.2 Diffuser-Thruster 11
    - 3.1.2.1 Torque 13
    - 3.1.2.2 Static Pressure 14
- 3.2 Circulation Control Tail Booms 15
  - 3.2.1 Fuselage Strakes 15
  - 3.2.2 Jet Slots 16
    - 3.2.2.1 Torque due to Boom Static Pressure Alone ... 17
    - 3.2.2.2 Torque due to Rotor Downwash Alone 18
    - 3.2.2.3 Torque due to Combined Effects of Circulation and Rotor Downwash 18
    - 3.2.2.4 Combined Effects 19

3.3 Infra-Red Suppression systems for helicopters 20
3.3.1 Perfect Mixer Performance Model 21
3.3.1.1 Mixer Performance 21
3.3.1.2 Diffuser Performance 22
3.3.1.3 Ejector Performance 22
3.3.1.4 Operating Point 23
3.3.2 Other Models 23
3.3.2.1 Momentum Integral Method 23
3.3.2.2 Finite Difference Method 24
3.3.3 Comanche - Example of Infra-Red Suppression System 25
3.4 Comments 25

4 Experimental equipment 26
4.1 Hot tests 26
4.1.1 Model 26
4.1.2 Burner 27
4.1.3 Fans 28
4.1.4 Instrumentation 28
4.2 Cold tests 30
4.2.1 Model 30
4.2.2 Blower 31
4.2.3 Fans 31
4.2.4 Instrumentation 32
4.3 Dual flow 33
4.3.1 Model 33
4.3.2 Fans, Blower 34
4.3.3 Instrumentation 34

5 Tests Procedures 36
5.1 Hot tests 36
5.2 Cold tests 36
5.3 Dual flow tests 37

6 Results and Discussion 39
6.1 Hot and Cold tests 39
6.1.1 Mass flow 39
6.1.2 Thrust 40
6.1.3 Power 42
6.1.3.1 Thruster 42
6.1.3.2 Fan 44
6.1.4 Static pressure 45
6.1.4.1 Fan air 45
6.1.4.2 Engine exhaust air 48
6.1.5 Temperature 50
6.1.5.1 Thruster Jet 50
6.1.5.2 Tail boom skin 52
6.2 Dual flow tests 53
6.2.1 Entrainment 53
6.2.2 Mass flow 54
6.2.3 Static pressure 54
6.2.3.1 Fan air 54
6.2.3.2 Engine exhaust air 55

7 Conclusions 57
7.1 Thruster 57
7.2 Fan Power 57
7.3 Static pressure 58
7.3.1 Fan air 58
7.3.1.1 Single flow system 58
7.3.1.2 Dual flow system 58
7.3.2 Engine exhaust gasses 59
7.3.2.1 Single flow system 59
7.3.2.2 Dual flow system 60
7.4 Temperature 60
7.4.1 Thruster Jet 60
7.4.2 Tail boom skin 61
7.5 Entrainment 61

8 Suggestions for further work 62
8.1 Pressure 62
8.1.1 Static pressure drop 62
8.1.2 Dual Flow Secondary Flow 62
8.2 Temperature 63
8.2.1 Single flow system 63
8.2.2 Dual flow system 64
8.3 Engine 64
8.4 Diffuser-Thruster 64

9 References 65

Appendix A A1
Calibrations of Equipment

Appendix B B1
Drawings of Model

Appendix C C1
Tables of results

List of Figures

Figure 1: Diagrammatic Arrangement of a Helicopter with CCTB&T Anti-Torque System 3
Figure 2: Diagrammatic Arrangement of a Helicopter fitted CIRSTEL 4
Figure 3: Diagrammatic Arrangement of Dual flow CIRSTEL system 5
Figure 4: General Arrangement of Thruster 8
Figure 5: Variation of Normalised Thrust with Can Angle 9
Figure 6: General Arrangement of Diffuser-Thruster 12
Figure 7: Variation of DT Thrust with Rotor Thrust 13
Figure 8: Static Pressure Distribution in Tail Boom 14
Figure 9: Diagrammatic Arrangement of Conventional Tail Boom with Strakes 15
Figure 10: Schematic Arrangement of Tail Boom with Jet Slots 17
Figure 11: Flow schematic and station identification of basis ejector 21
Figure 12: Diagrammatic Arrangement of set-up for hot tests 26
Figure 13: Photograph of Burner in HGTF 27
Figure 14: Diagrammatic Arrangement of set-up for cold tests 31
Figure 15: Diagrammatic Arrangement of Dual flow test rig 34
Figure 16: Diagrammatic Arrangement of set-up to measure entrainment 38
Figure 17: Control Volume across thruster 40
Figure 18: Variation of Thruster thrust with (Apt)thr 41
Figure 19: Variation of Thruster Power with T3/2/(Arho)^0.5 43
Figure 20: Variation of Kpfan with Velocity ratio 44
Figure 21: Control Volume across tail boom 46
Figure 22: Variation of function f with mass flow ratio 47
Figure 23: Variation of function g with mass flow ratio 49
Figure 24: Variation of Tf with mass flow ratio 51
Figure 25: Variation of tail boom surface temperature with mass flow ratio 52
Figure 26: Variation of entrainment ratio with blower flow 53
Figure 27: Variation of function f with velocity ratio for dual flow system 55
Figure 28: Variation of function g with velocity ratio for dual flow system 56

List of Tables

Table 1: Instrumentation for hot tests 28
Table 2: Instrumentation for cold tests 32
Table 3: Instrumentation for dual flow tests 34
Table C1: Results of hot tests : 4 fans running C2
Table C2: Results of hot tests : 3 fans running C3
Table C3: Results of hot tests : 2 fans running C4
Table C4: Results of cold tests : 4 fans running C5
Table C5: Results of cold tests : 3 fans running C6
Table C6: Results of cold tests : 2 fans running C7
Table C7: Results of dual flow tests : At/Ab = 0.62 ..... C8
Table C8: Results of dual flow tests : At/Ab = 1.02 ..... C9
Table C9: Results of dual flow tests : At/Ab = 1.22 ..... C10
Table C10: Results of dual flow tests : At/Ab = 1.48 ..... C11
Table C11: Results of entrainment measurements C12

1 Introduction

1.1 Background

The function of the tail rotor of a helicopter (with the single main rotor and tail rotor configurations) is to counteract the torque applied to the main rotor. The torque applied to the main rotor is a function of a number of factors including its lift and forward speed. This means that the amount of torque produced by the tail rotor must vary to counteract this changing torque. The torque provided by the tail rotor must also be variable to provide yaw control to the helicopter.

The conventional tail rotor, introduced in 1939, has a number of disadvantages. It is a mechanically complex system that requires a drive shaft mechanism from the main rotor gearbox and also a collective pitch mechanism. It is also susceptible to damage, noisy ,dangerous, and intolerant to battle damage.

Two other systems that have been developed to replace the conventional tail rotor are the fenestron [1] and the circulation controlled tail boom and thruster. [2] The fenestron comprises of a shrouded tail rotor. The shroud eliminates the trailing vortices and the consequent contraction of the wake and consequently results in a reduced power for a given rotor disc area. The shroud also protects the rotor from mechanical damage, increases safety, and reduces noise. The fenestron has been implemented by Areospatiale on for example the Gazelle and Dauphin helicopters.

1.2 Circulation controlled tail boom and thruster

The circulation control tail boom and thruster (CCTB&T) develops the anti-torque requirements of the helicopter by means of three effects. The first is circulation control. Air is blown through slots cut along the length of the tail boom. This air adheres to the surface of the tail boom (due to the COANDA effect, see reference [3]), flowing around the tail boom for approximately 180°. This generates circulation around the tail boom. This circulation combined with the downwash from the main rotor generates a force that is normal to the direction of flow of the downwash from the main rotor, resulting in a torque acting about the main rotor axis. The CCTB is most effective at low forward speed in the order of a few meters per second.

The second effect is a thruster fitted to the end of the tail boom that produces a torque by turning the air through approximately 90° and then exhausting it into atmosphere. This force acting at the end of the tail boom produces a torque that counteracts that of the main rotor. The torque developed by the thruster can be altered by varying the outlet area of the thruster and the total pressure of the air.

The third effect is two vertical tail fins that are fixed to the tail boom. These fins are most effective at high speeds. The angle of incidence of at least one of the vertical fins is controllable.

The CCTB&T has been implemented by McDonnell Douglas Helicopter Company on their MD520N and MDX helicopters. [4]

The CCTB&T has a number of advantages when compared to the conventional tail rotor. The effect of tail rotor strikes and hazards to personnel are reduced. The tail boom is less susceptible to enemy fire. This is mainly because the

driveshaft and gearbox are eliminated from the tail boom. The fan is situated in the body of the helicopter and requires only a short driveshaft.

Vibration and Noise is also reduced. Noise levels on the MD520N were measured to be on average from 2,7 to 7dB [5] quieter (when compared on a weight corrected basis) than the MD500E, depending on the flight condition. The MD520N was shown to be significantly quieter than all tail rotor-equipped helicopters certified to date.

A general arrangement of a helicopter fitted with a CCTB&T appears in figure 1

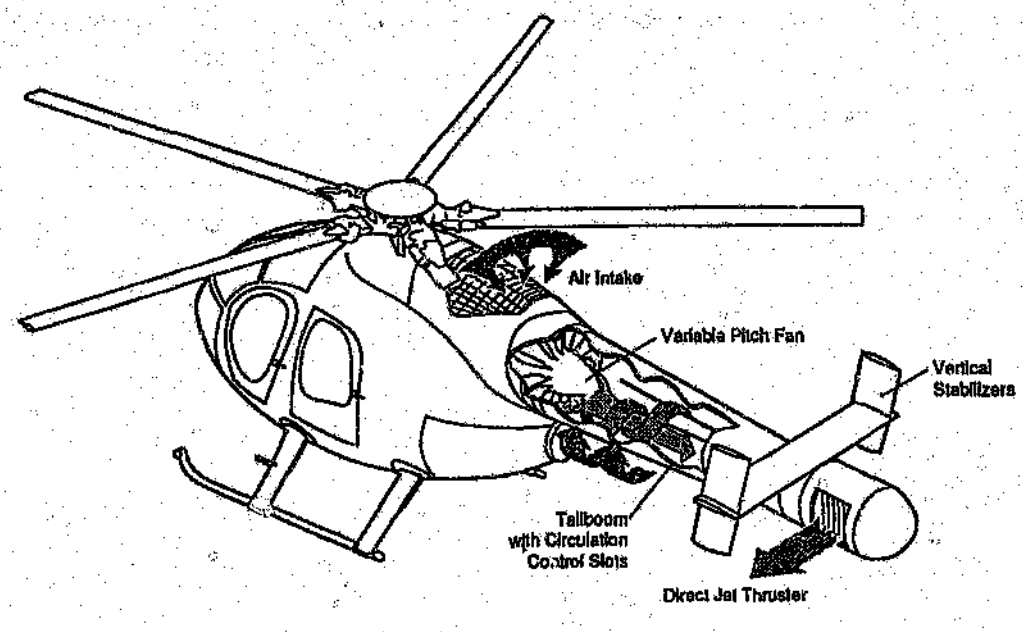


Figure 1: Diagrammatic arrangement of a Helicopter with CCTB&T Anti-Torque System [4]

1.3 Combined Infra-red suppression and tail rotor elimination

The temperature of the exhaust gases of a helicopter is in the region of 500 °C. This offers a significant infra-red signature to heat seeking missiles. Combined Infra-Red Suppression and Tail rotor ELimination (CIRSTEL) is a concept that

utilises the ambient air, that is used in the CCTB&T system, to cool the engine gases before they are exhausted into the atmosphere. Two ways of doing this are possible.

1.3.1 Single flow system

The first system exhausts the hot engine gases into a mixing tube that is situated in the tail boom. A single fan then supplies air to both the CCTB and the thruster. A portion of the ambient air supplied by the fans mixes, inside the mixing tube, with the hot air from the engine. The rest of the ambient air supplied by the fans passes on the outside of the mixing tube to supply air to the circulation control slots. The air that does not exhaust through the circulation control slots then mixes with the air exhausting from the mixing tube. This final mixture of air is then exhausted through the thruster. A diagrammatic arrangement of a helicopter fitted with a CIRSTEL system is given in figure 2.

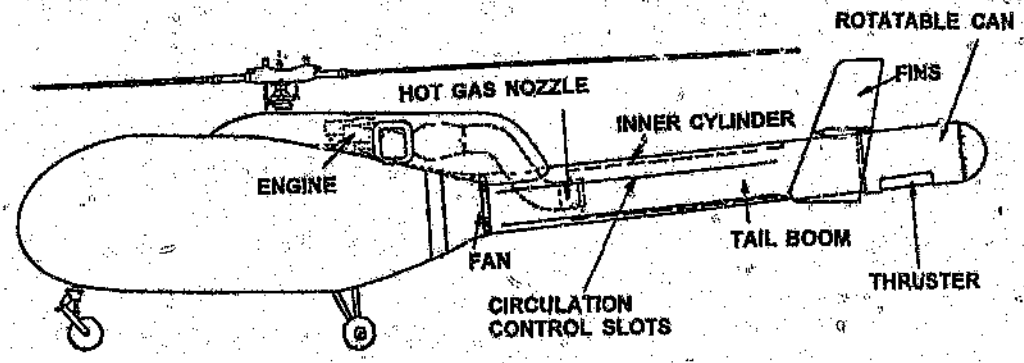


Figure 2: Diagrammatic Arrangement of a Helicopter fitted with CIRSTEL [6]

1.3.2 Dual flow system

The other possibility is to have two separate flow paths with different total pressures. The air supplied to the thruster needs to have a high mass flow rate, but a low pressure. The air that is supplied to the circulation slots needs to have a low mass flow rate but a high pressure. The dual flow system will supply low pressure air to the thruster at a high mass flow rate and high pressure air to the circulation control slots at a low mass flow rate. This can be done with either having two separate fans or a single fan that can supply the two flows. This will have the advantage that the power requirements of the system will be reduced (when compared with the single flow system) due to the lower pressure of the air that is supplied to the thruster.

This will also mean that only the air going to the thruster will mix with the hot air from the engine. The air going to the circulation control slots would then ensure that the outer wall of the tail boom will remain at a low enough temperature not to produce a significant infra-red signature. A diagrammatic arrangement of a dual flow CIRSTEL system appears in figure 3

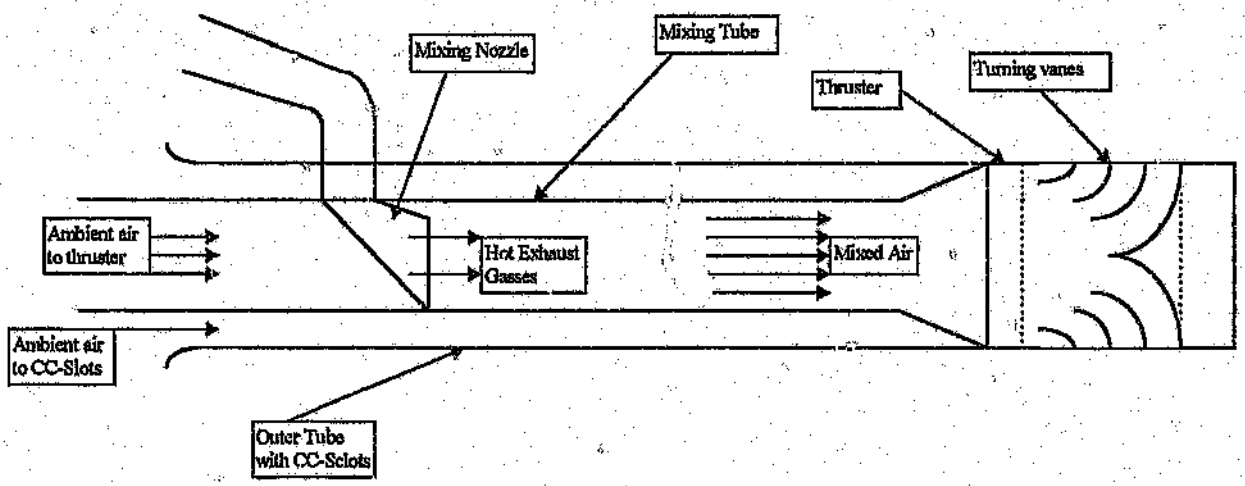


Figure 3 :Diagrammatic arrangement of Dual flow CIRSTEL system

2 Objectives

The main objective of this research program was to investigate and characterise the performance of a CIRSTEL system. This was achieved by:

1. Designing and building half scale models of the two CIRSTEL systems,

2. Investigating the effect of the mixing nozzle on the performance of the CCTB&T system by studying the effect in the power required from the fan supplying ambient air to the CCTB&T system, as well as the drop in static pressure of both the air flow from the fans and the flow from the engine,

3. Comparing the performance of the Dual flow and Single flow systems in terms of the drop in static pressure of the flows from the fans and the engine.

4. Studying the effect of temperature on the system by testing with both hot and cold air to simulate the engine exhaust gasses,

5. Studying the performance of the thruster on the CCTB&T system and comparing data obtained with data from tests done at the University of the Witwatersrand.

5. Investigating the effectiveness of the CIRSTEL concept in terms infra-red suppression (cooling of engine exhaust gasses).

3 Literature Survey

No literature was found on Combined Infra-Red Suppression and Tail Rotor Elimination (CIRSTEL) systems for helicopters. The literature survey therefore concentrates on the following three components of the CIRSTEL system:

1: Jet thrusters
2: Circulation Control Tail Booms
3: Infra-Red Suppression systems for helicopters

3.1 Jet Thrusters

During the entire forward flight envelope it is the vertical fins fitted to the CCTB that develops most of the torque to counter-act the torque applied to the main rotor. The thruster is used to supplement and trim the torque developed the CCTB during hover and sideways flight as well as the forward flight envelope. It is therefore essential that the performance of the thruster be characterised in terms of power and torque developed.

Tests were carried out on two different options of replacing the conventional tail rotor at the University of the Witwatersrand (See references 7 and 8). The first is the Circulation Control tail boom and Thruster (CCTB&T). The performance of the thruster was tested on a static rig situated at the laboratory of the School of Mechanical Engineering of the University of the Witwatersrand. These tests were used to determine the operation of the thruster as well as the variation of the thrust developed by the thruster with variation in exit area of the thruster. The exit area of the thruster was varied by rotating a can (with an opening larger than that of the thruster) around the thruster. Another method of varying the outlet area of the thruster is by means of a slide. The main advantage of the slide is that the air exhausting from the thruster is not deflected in the vertical

direction as in the case with the rotating can. See figure 4 for a general arrangement of the thruster with a rotating can.

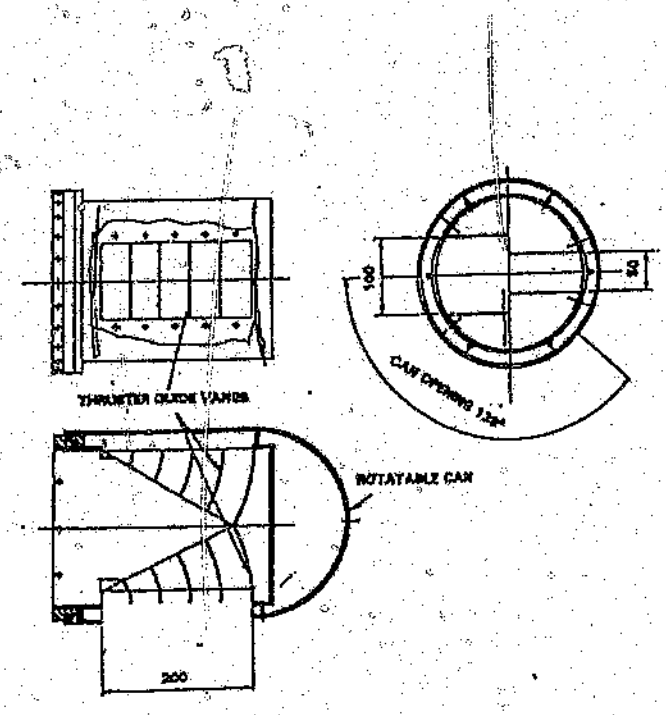


Figure 4: General Arrangement of Thruster

3.1.1 CCTB&T

3.1.1.1 Thrust

The variation of the normalised thrust developed by thruster with can angle is presented in figure 5. It is clear that thrust developed by the thruster can easily by controlled by varying the angle of the outer can.

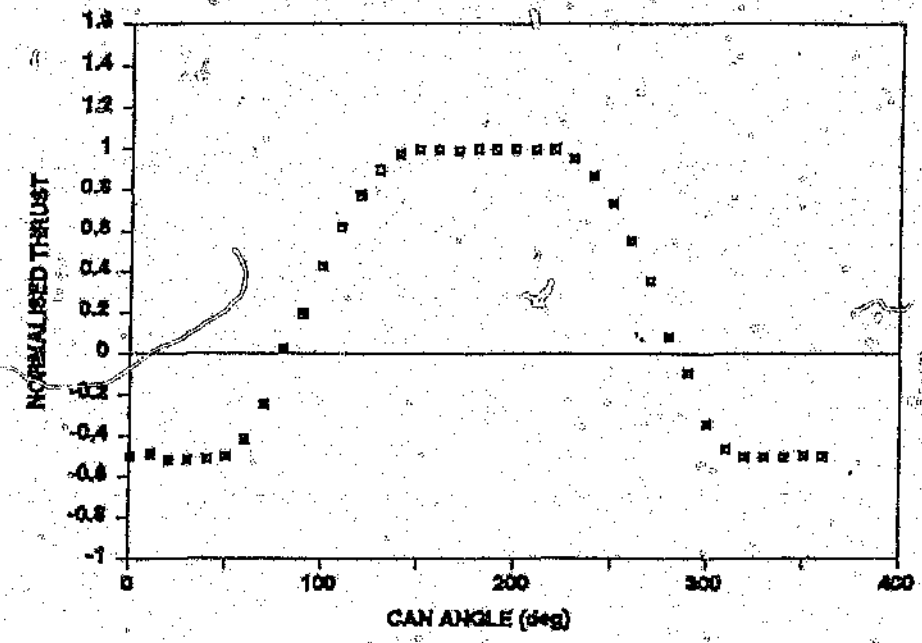


Figure 5: Variation of Normalised Thrust with Can Angle [7]

Using conservation of momentum across the thruster gives:

$$\Sigma F = G_f(V_f - V_t) + A_t(P_f - P_a) \qquad 3.1$$

Assuming $V_t = 0$, equation 3.1 can be given as:

$$T_T = k_1 A P_t \qquad 3.2$$

Unknown factors such as velocity components in the tail boom, non-uniform flow and expansion of the wake are included by means of the constant k_1.

From this it is clear that the torque developed by the thruster about the main motor is given by:

$$Q_t = k_1 A P_t L_t \qquad 3.3$$

where L_t is the horizontal distance from the main rotor axis to the mid point of the exit area of the thruster.

For the tests carried out at the University of the Witwatersrand it was found that the value of the constant k_1 is 1,0757 for the geometry tested. The thrust developed by a thruster with a similar geometry to the thruster tested in reference 7 can thus be written as:

$$T_T = 1{,}0757 A P_t \qquad 3.4$$

Later tests has shown the value of k_1 is in fact a function of the area ratio of the thruster [9]. The value of k_1 decreases as the area ratio of the thruster increases. No tests were carried out to determine the effect the geometry of the thruster has on the value of the constant k_1.

3.1.1.2 Power

The power supplied to the thruster for the case of no frictional losses may be given by:

$$P = K_p \frac{T^{3/2}}{(A\rho)_{thr}^{0.5}} \qquad 3.5$$

where $K_P = 0,5$.

The power supplied to the fan to provide the air to the thruster may be written as:

$$P = K_p \frac{T^{3/2}}{(A\rho)_{thr}^{0.5}} \qquad 3.6$$

where K_P includes the effects of energy losses due to friction, variation in the cross-section of the jet leaving the thruster, and the fan efficiency.

For the tests carried out at the University of the Witwatersrand [7] it was found that $K_P = 0,856$. Further tests [9] at the University o the Witwatersrand has shown that K_P is in fact a function of the area ratio of the thruster. The value of K_P increases with an increase in the area ratio. What is not shown in these tests is the dynamic response of the air flow to the opening or closing of the thruster exit.

3.1.2 Diffuser-Thruster (DT)

The Diffuser-Thruster is the second option for replacement of the conventional tail rotor that was tested at the University of the Witwatersrand [8]. The DT comprises of:

i) a fan located at the entrance to the tail boom
ii) a tail boom to duct air from the fan to it's aft end
iii) a diffuser located at the aft end of the duct to reduce the speed of the air, and
iv) a thruster fitted to the outlet of the diffuser which turns the air through approximately 90° and ejects it sideways with a nearly uniform exit

velocity to generate a thrust and consequently the torque required to balance that applied to the main rotor.

See figure 6 for a general arrangement of a Diffuser-Thruster.

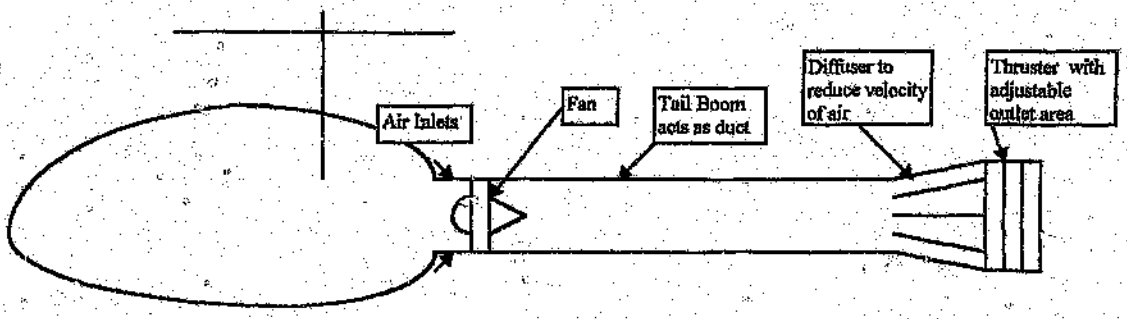


Figure 6: General Arrangement of Diffuser-Thruster

The DT has two main advantages over the CCTB&T concept. The first is the fact the Circulation Control Tail Boom only functions properly at hover or very low forward speeds. At higher forward speed, as the main rotor downwash moves off the tail boom, the CCTB loses its effectiveness.[10] As no circulation control is used on the DT the problem should not occur.

The static pressure of 7kPa [8] inside the tail boom of the CCTB results in an exit velocity of approximately 105m/s. This velocity is high compared to that of the conventional tail rotor or the fenestron and results in comparatively high power requirements for the thruster. The overall power requirements of an anti-torque system comprised of a circulation controlled tail boom and thruster appears to be in the order of 50% higher than that of a conventional tail rotor [9]. If the speed (total pressure) of the air could be reduced before exiting through the thruster it could be possible to reduce the power requirements of the system significantly.

It is also clear from equation 3.6 that the power consumption of the CCTB&T is a function of the outlet area of the thruster. If the outlet area of the thruster could be increased it would mean that the power requirements would also be reduced.

The fact the mass flow through the DT will be significantly higher than that of the CCTB&T (10 kg/s for the CCTB&T versus +- 29 kg/s for the DT) could mean that the DT could be a better option for the CIRSTEL concept. The higher mass flow of ambient air would mean that the temperature of the engine exhaust gasses would be further reduced than would be the case of the for the CCTB&T.

A number of problems are still associated with the current design of the DT. It was therefore decided to use the CCTB&T for this study.

3.1.2.1 Torque

The tests carried out on the DT a the University of the Witwatersrand were done on both a static rig and the rotor spin rig. The tests on the rotor spin rig clearly showed that in hover the rotor has limited effect on the torque developed by the DT. See figure 7.

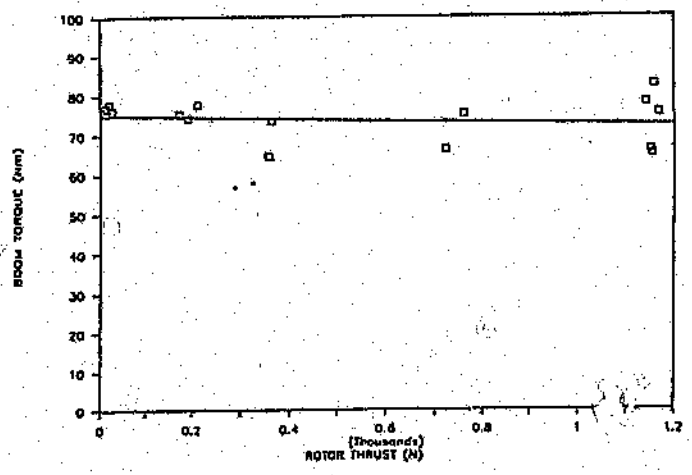


Figure 7: Variation of DT Thrust with Rotor Thrust [8]

3.1.2.2 Static Pressure

As one of the possible uses of the DT would be the cooling of exhaust gasses by passing them through the tail boom, it was pertinent to investigate the static pressure existing in the tail boom. Figure 8 presents the static pressure along in the tail boom of the CCTB and the two DT's that were tested. The static pressure depressions on the tail boom for the two DT's are significant. This static pressure depression combined with the large flow of ambient air would be useful for drawing exhaust gasses in to the tail boom.

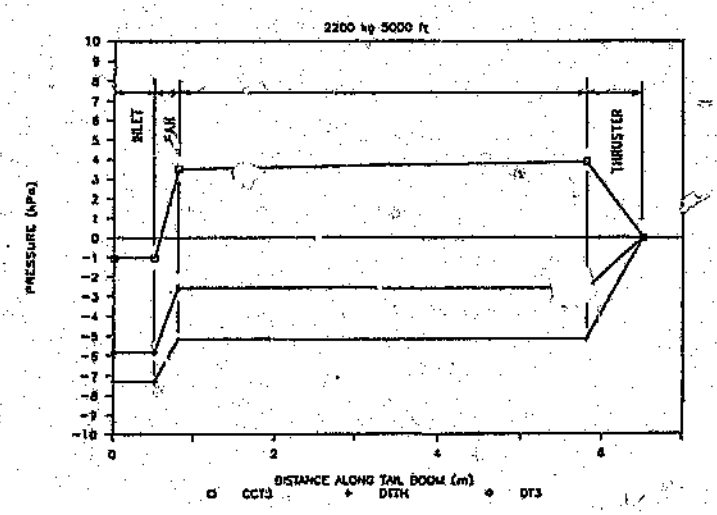


Figure 8: Static Pressure Distribution in Tail Boom [8]

The results from the tests carried out on the DT show that its thrust performance compares favourably with that of the conventional tail rotor. Further work is still

required to improve performance and to ensure that the mass penalty is acceptable. The flow in the in the diffuser and the thruster can be improved. This would mean a reduction in the losses and improved performance of the DT.

3.2 Circulation Control Tail Booms

Circulation control tail boom anti-torque systems make use of the downwash from the main rotor and an induced circulation around the tail boom to generate a torque about the axis of the main rotor. This circulation can be induced by means of two separate mechanisms.

3.2.1 Fuselage Strakes

This mechanism makes use of strakes (flaps) mounted on the fuselage of the helicopter [11]. See figure 9. The strakes alter the air flow around the tail boom by separating the flow from the boom. This reduces the velocity of the air on the one side of the boom producing circulation, which, when combined with the downwash from the main rotor, creates a lateral air load to oppose the main rotor torque.

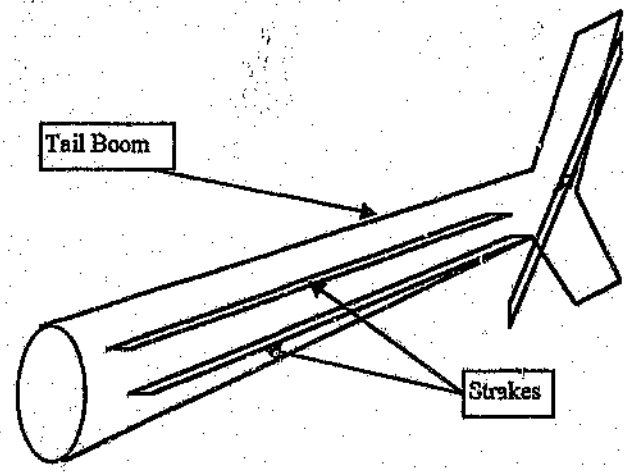


Figure 9: Diagrammatic arrangement of conventional tail boom with strakes

This arrangement has the following advantages:

i) Reduces the load requirements on the helicopter torque control systems,
ii) Reduces the size of the torque control system by using the fuselage air loads to provide part of the needed torque,
iii) Increases the sideslip ability of the helicopter by controlling the flow circulation around the fuselage and
iv) With retractable/extendible strakes the performance of the strakes can be optimised.

Although the increase in torque developed by the strakes is only in the region of 10% [9] of the torque developed by the conventional tail rotor, all of the above mentioned advantages can be obtained with no requirements in engine power, internal ducting or drive mechanisms. Due to the reduction in loads on the torque control system, the maintainability and reliability of the helicopter is also improved at very small cost.

The reduction in the size of the torque control system will mean reduced drag and weight. This will mean increased performance through increased speed, increased fuel savings and increased load capacity.

3.2.2 Jet Slots

The second mechanism to induce circulation around the tail boom is to cut jet slots along the length of the tail boom. Air, supplied by an axial fan, is then ducted through the tail boom at a positive pressure relative to atmosphere. The air is then exhausted, tangential to the boom surface, through the jet slots. The air has sufficient energy to stay attached to the surface due to the COANDA effect for a considerable distance(upto 270° from the vertical). This distance that the air stays attached to the surface of the tail boom can be controlled by making

use of he fuselage strakes mentioned in 3.2.1. The effect is that a circulation is set-up around the boom and in combination with the downwash from the main rotor produces a torque to counter-act the torque applied to the main rotor. See figure 10.

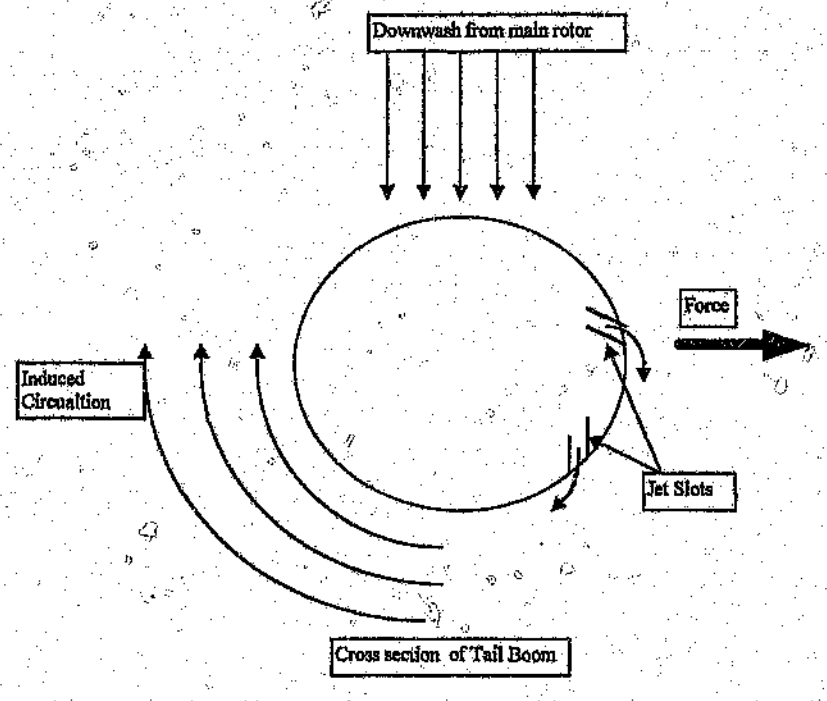


Figure 10: Schematic diagram of Tail Boom with Jet Slots

3.2.2.1 Torque due to Boom Static Pressure Alone

For the case where there is no rotor downwash, the torque acting on the tail boom can be given by [12]:

$$Q_1 = k_3(L_2^2 - L_1^2)P_s t = k_3(L_2^2 - L_1^2)P_s(t/D)D \qquad 3.7$$

where k_3 includes the frictional losses on the surface of the tail boom.

This torque is produced by the horizontal component of the change of momentum of the air leaving the surface of the tail boom. The effect of the of the diameter of the tail boom could be determine in terms of the Reynolds number based on the boom diameter [12]. Results of tests presented in reference 12 show that k_3 is independent of this Reynolds number. Data from references 9 and 12 indicate that $k_3 = 0{,}462$ (for D = 0,299m). Whether k_3 is in fact independent of the boom diameter still has to be determined experimentally.

3.2.2.2 Torque due to Rotor Downwash Alone

Perturbations on the surface of the tail boom result in the rotor downwash flowing asymmetrically around the tail boom thereby [illegible]culation. This circulation combined with the rotor downwash produ[illegible]force[illegible]s is the same effect as the fuselage strakes discussed in 3.2.1. The direction and magnitude of the force will depend on th[illegible] perturbation on the surface of the tail boom. This component of the torque is given by:

$$Q_2 = k_4 TD \qquad 3.8$$

where $k_4 = 0{,}05943$ (see references 9 and 12)

3.2.2.3 Torque due to Combined Effects of Circulation and Rotor Downwash

When both the downwash and circulation control is used a force and torque is developed that acts about the axis of the main rotor. It has been shown in 9 and 12 that this torque component is proportional to the rotor thrust and the square root of the static pressure in the tail boom. Unpublished results show that this component of torque is also proportional to the diameter of the tail boom. This component of may be written as:

$$Q_3 = k_5 P_s^{1/2} TD \qquad 3.9$$

where k_5 = 0,00561(from references 9 and 12)

It has been shown in references 9 and 12 that the three components of torque are additive, i.e. the total torque acting on the tail boom is:

$$Q = Q_1 + Q_2 + Q_3 \qquad 3.10$$

3.2.2.4 Combined Effects

From 3.2.2.3 the total torque developed by the circulation control tail boom is given by:

$$Q = 0{,}462(L_2^2 - L_1^2)P_s(t/D)D + 0{,}05943TD + 0{,}00561\, P_s^{1/2} TD \qquad 3.11$$

The total power applied to the fan is given by:

$$P = [(G - G_T)/\rho](P_t/\eta) + k_2[T^{3/2}/(\rho A)^{1/2}] \qquad 3.12$$

3.3 Infra-Red Suppression systems for helicopters

(See references 6 and 13)

The hot gasses exhausted from the engine of a helicopter, as well as the components that the hot gasses comes in contact with, provide a significant signature to infra-red guided missiles. The methods that are employed to reduce this infra-red signature are the masking of hot areas and the cooling of the hot engine gasses by combination thereof with cold air before exhausting it into atmosphere.

The first generation suppressors feature an upward bent nozzle shielded from enemy view by an insulating cowl. This concept is adapted for apposing band 1 operated missiles (wavelength = 1,7 to 2,8μm). Exhaust plumes radiate a detectable amount of energy due to discreet rays in the carbon dioxide spectrum, a part of which is included in band 2 (wavelength = 3,7 to 4,8μm). Diluting the exhaust gasses with cold ambient air reduces the concentration of CO_2 and the temperature and therefore reduces the detecability of the aircraft.

A basic ejector consists of the flowing four components (See figure 11):

1) Primary nozzle : To inject hot engine exhaust gasses in to mixing duct, at station 1
2) Intake : To collect , direct and accelerate ambient air upto station 2
3) Mixing duct : where momentum is transferred from primary to secondary stream and the two flows are mixed under the action of turbulent friction.
4) Diffuser : where the residual kinetic energy is partially recovered in transformed into pressure.

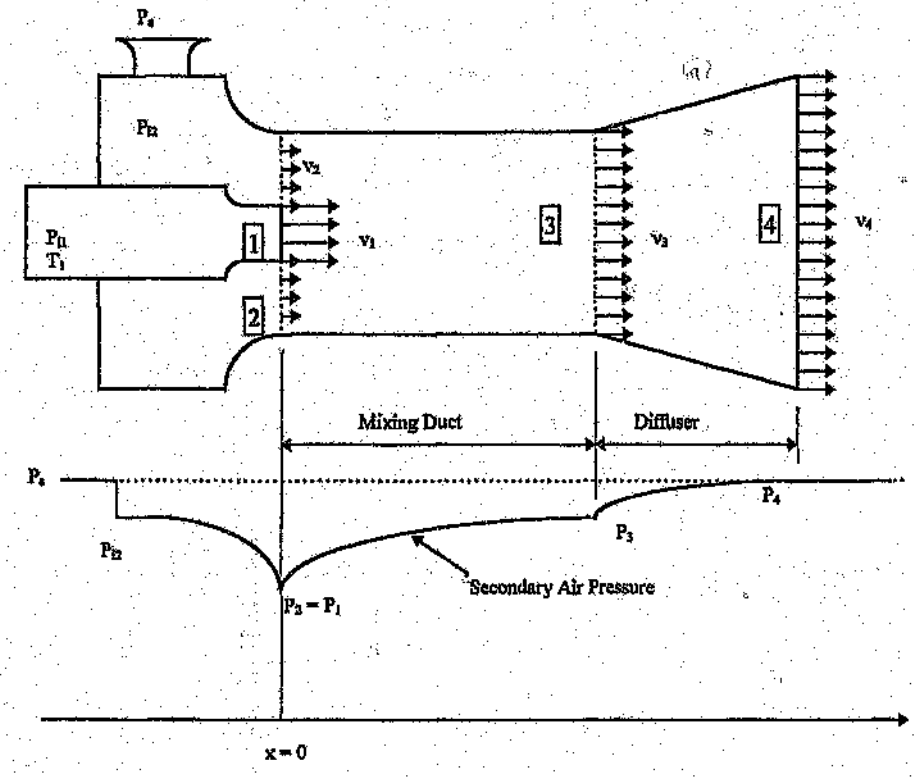


Figure 11: Flow schematic and station identification of basic ejector

3.3.1 Perfect Mixer Performance Model

3.3.1.1 Mixer Performance

Making the following assumptions:

1) The mixer is long enough to achieve complete transfer of momentum from primary to secondary flow,
2) Momentum lost on the wall boundary layer can be neglected and
3) The flow is homogeneous over any section 1,2 or 3 (boundary layer thickness is neglected),

the static pressure rise from station 2 to 3 can be expressed as a function of the area ratio λ ($(A_1 + A_2)/A_1$), the temperature ratio θ (T_1/T_2), and the corrected flow ratio Φ', ($(F_2/F_1)/\sqrt{\theta}$):

$$(P_3 - P_2)/q_1 = 2(\lambda - 1)/\lambda^2(1 - 2f_\theta(\Phi'/(\lambda - 1)) + (\Phi'/(\lambda - 1))^2) \quad 3.13$$

where $f_\theta = (1 + \theta)/2\sqrt{\theta}$ is an auxiliary temperature function.

3.3.1.2 Diffuser Performance

The performance of the diffuser may be defined as:

$$\eta_d = (P_a - P_3)/q_3 \quad 3.14$$

3.3.1.3 Ejector Performance

The pressure rise achieved by the complete ejector is obtained by summing up the mixer and diffuser contributions:

$$(P_a - P_2)/q_1 = \omega = 2(\lambda - 1)/\lambda^2(1 - 2f_\theta(\Phi'/(\lambda - 1)) + (\Phi'/(\lambda - 1))^2) + \eta_d((1 + 2f_\theta \Phi' + \Phi'^2)/\lambda^2) \quad 3.15$$

An equivalent expression for head pressure is:

$$(P_a - P_{t2})/q_1 = \Pi = \omega - (\Phi'/(\lambda - 1))^2 \quad 3.16$$

Plotting the Pressure rise, Π, corrected flow rate, Φ', gives the so called ejector performance curve. This curve is dependent on the geometry of the ejector but nearly independent of the Mach number and Reynolds number [13].

3.3.1.4 Operating Point

The operating point is determined by matching the ejector pressure rise to the pressure loss of the intake system. The pressure loss varies with the dynamic pressure of the secondary flow rate q_2:

$$P_a - P_{i2} = k_2 q_2 \qquad 3.17$$

The coefficient k_2 does not significantly vary within the usual range of Reynolds numbers (fully turbulent flow). Therefore:

$$\Pi = k_2 (\Phi'/(\lambda - 1)) \qquad 3.18$$

The operating point of the ejector rests at the intersection of equations 3.16 and 3.18. It was found that the neither the velocity v_1 nor the cross section shape has any influence on the flow ratio as long as λ is retained. It was however found that the nozzle shape does have an influence when the above hypothesis is proven wrong.

3.3.2 Other Models

3.3.2.1 Momentum Integral Method

(See reference 13)

The most unrealistic assumption introduced in the perfect mixer model is the complete transfer of momentum. The mixer is seldom longer than the diameter of the infra-red suppressor so that the velocity profile is far from uniform at station

3. This limitation tends to reduce the pressure rise. The non-uniformity of the flow resulting from non-perfect mixing lowers the diffuser efficiency. The diffuser pressure rise is therefore also reduced. On the whole, the ejector performance falls short of the perfect mixer curve. In order to predict the pressure rise of a short ejector, it is necessary to know the residual momentum integrated over the end of cross section 4. This in turns depends on the velocity profile at station 4.

3.3.2.2 Finite Difference Method

(See reference 13)

In contrast to the preceding method, this method does not rely on any kind of flow similarity, but solves the local equations of continuity, longitudinal momentum and energy. The equations take the conventional boundary layer form whose main features are:

1) quasi-parallel streamlines, no separation or reversed flow,
2) constant pressure over any cross section and
3) no influence of the downstream region onto the upstream flow.

The finite difference method has two advantages over the previous method:

1) The effect of wall friction is properly included, a crucial point for the calculation of diffusing ducts.
2) Heat transfer and compressibility are accounted for within the state and energy equations.

It should be noted that the finite difference method is doomed to fail at point of separation.

An example of infra-red suppression is used on the Comanche [14] which, although it makes use of a fenestron anti-torque system, mixes the hot engine exhaust gasses with cooler ambient air inside the tail cone. This mixture then passes through long ribbon diffusers located on each side of the tail cone, where it exits through 15-foot by 4-inch slots on either side of the tail cone. As it escapes, the warm air is further mixed with the downwash from the main rotor.

3.4 Comments

Although the above mentioned methods were available to characterise the infra-red suppression performance of the CIRSTEL system, it should be noted that none of them were intended to be applied in the set-up as used in the CIRSTEL system where the ambient air is forced through the system at high pressure. Even when used in the application that they where intended for, the methods still have a number of shortcomings. Additional factors such as inlet distortions and duct curvatures may affect the performance of the suppressor.

A much easier method, which relates the drop static pressure of the flow from the fans and the flow from the engine to the velocity or mass flow ratio, was devised to predict the static pressure of the two flows. This method was rather used for the tests in this program.

The same thrust and power coefficients used for the tests at the University of the Witwatersrand was used for the tests conducted in this program. This made the comparison of data easier.

4 Experimental equipment

4.1 Hot tests

4.1.1 Model

A half scale CIRSTEL model was used for the hot tests. A diagrammatic arrangement of the model and the test facility are presented in figure 12.

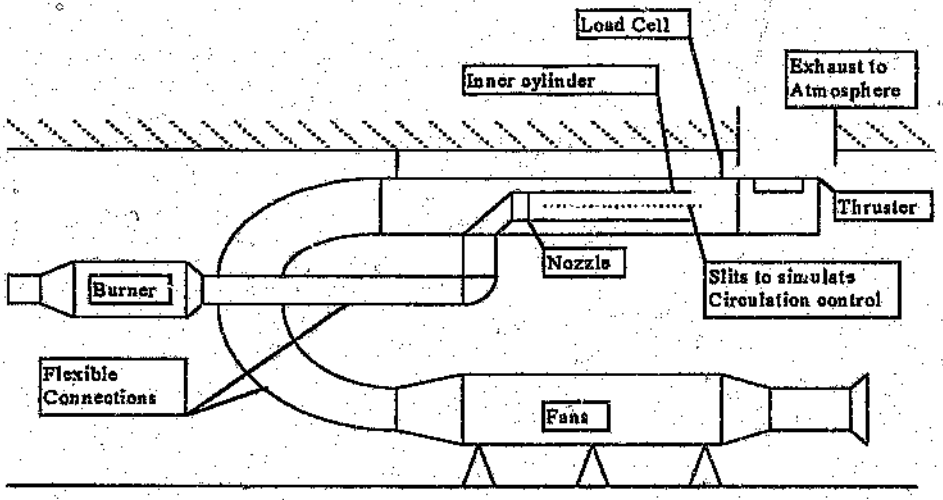


Figure 12: Diagrammatic arrangement of hot test set-up

The model for the single flow system consists of a 300mm diameter pipe with a length of 2,3m. Two slots are cut along the length of the pipe to simulate the circulation control slots. These slots do not generate any circulation (or torque) but only exhaust approximately the same amount of air (to scale) that would be exhausted by the circulation control slots on the full scale model. Inside the 300mm tube is placed a 260mm diameter tube. The hot air used to simulate the engine exhaust gases are ducted into the model and then exhausted into the 260mm mixing tube through a mixing nozzle. The mixing nozzle is an

asymmetrical daisy nozzle with an average diameter of 250mm and an outlet area of 0,0249m^2. A thruster is fitted to the end of the 300mm tube. The thruster has two outlets of differing sizes. Blades inside the thruster help to turn the air before it is exhausted into the atmosphere. A can fits over the thruster. It is possible to rotate the can and thereby vary the outlet area of the thruster. The direction of thruster can also be reversed by closing off the outlet on the one side of thruster and opening the outlet on the other side of the thruster.

4.1.2 Burner

The burner at the Hot Gas Test Facility (HGTF) of the Council for Scientific and Industrial Research was used to supply the hot gasses to simulate the engine exhaust gases. The burner can supply upto 3,5 kg/s of air at upto 700 °C. The mixing nozzle was connected to the burner with a flexible bellows. This was done to ensure that the model was free to move in all directions and the load cell readings were not affected. See figure 13 for photograph of burner.

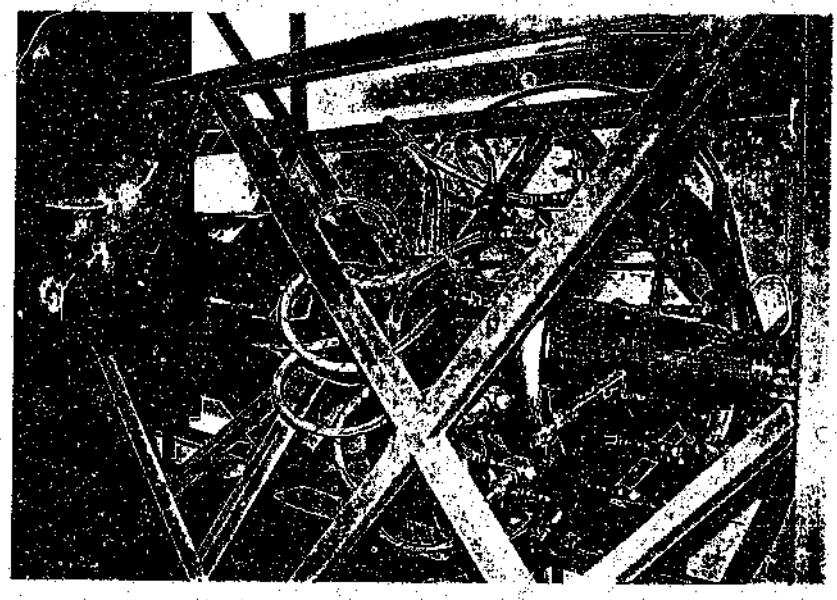


Figure 13 : Photograph of burner in HGTF

4.2.3 Fans

A set of four axial fans, connected in series, was used to simulate the ambient air flow in the model. Each fan could be switched on individually. This made it possible to have either 2,3 or 4 fans switched on at a time. The fans were installed next to the model. The air was then ducted into the model with a metal reinforced fabric concertina pipe.

With ideal conditions these fans can deliver upto 4 kg/s of air, but due to losses in the concertina pipe it was only possible for the fans to deliver a maximum of 2,1 kg/s of air. This is only half the air that is required for half scale tests. This was compensated for by also varying the flow from the burner, thereby producing the correct flow ratio and ensuring that the characterisation of the performance of the CIRSTEL system could be applied over a wide range of flow ratios.

4.1.4 Instrumentation

Instrumentation fitted to the test rig is given in table 1.

Table 1: Instrumentation for hot tests

□	Parameter	Sensor	Range	Std Dev
1	Thruster thrust	Strain gauge load cell	500N	6,75N
2	Temperature of air flow to burner	Thermocouple probe	800°C	2%
3	Temperature of air flow from burner	Thermocouple probe	800°C	2%
4	Temperature of air at mixing nozzle	Thermocouple probe	800°C	2%

5	Temperature of air at circulation slots	Thermocouple probe	800°C	2%
6	Temperature of air from fans	Thermocouple probe	800°C	2%
7	Temperature of air at thruster outlet	Thermocouple probe	800°C	2%
8	Velocity head of air from fans	Anubar + differential pressure transducer	30" WC	0,06 mB
9	Static pressure of air to burner	Anubar + differential pressure transducer	50 psi	0,524 mB
10	Velocity head of air to thruster	Anubar + differential pressure transducer	0,5 psi	5,34 mB
11	Static pressure of air from fans	Anubar + differential pressure transducer	50 psi	0,351 mB
12	Total pressure of air to burner	Anubar + differential pressure transducer	4 bar	10,9 mB
13	Total pressure of air to thruster	Anubar + differential pressure transducer	50 psi	1,01 mB
14	Static pressure of ambient air around mixing nozzle	Scani Valve	1 psi	6.54 Pa
15	Static pressure of engine air inside mixing nozzle	Scani Valve	1 psi	6.54 Pa

16	Static pressure of ambient air before mixing nozzle	Scani Valve	1 psi	6.54 Pa

The pressure transducers, scani valve and temperature probes were read by making use of a MUX-card connected to a personal computer. The software used was specifically developed for the test rig at the HGTF. The software was used to calculate the flow rates using the pressures read from the anubars. This made it possible to monitor the flow rates from both the fans and the burner and to set the flow ratio to the required value. Data read during the tests were saved as an ASCII file to be processed later.

4.2 Cold Tests

4.2.1 Models

The tests carried out in the HGTF were repeated for the cold tests to determine whether the performance coefficients are a function of the density of the gases in the tail boom. This time however the hot gas from engine was simulated with a blower delivering air at ambient temperature to the mixing nozzle. The same model was used as in the hot tests. The mixing nozzle was now connected to the blower (instead of the burner) by means of a short piece of metal reinforced fabric concertina pipe. The model was suspended in a scaffolding structure. A diagrammatic arrangement of the set-up is presented in figure 14.

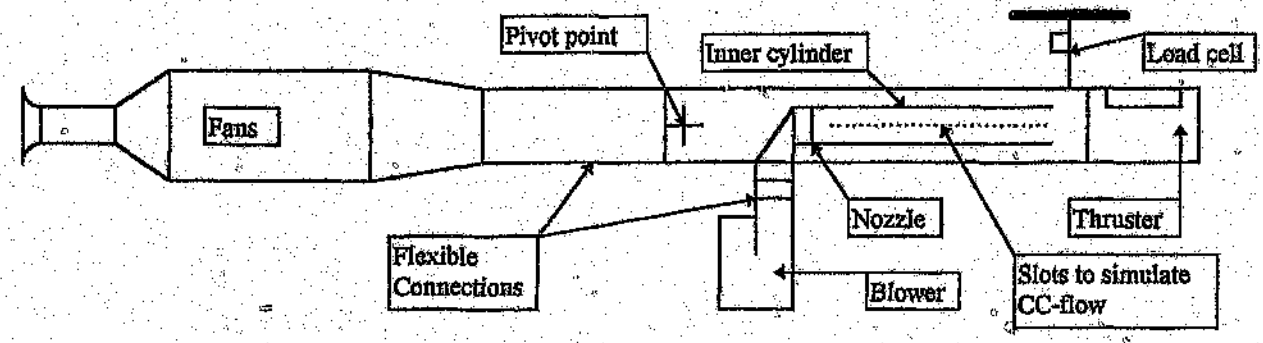


Figure 14: Diagrammatic arrangement of cold test rig

4.2.2 Blower

For the cold tests the engine flow was simulated by making use of a radial blower to supply air to the mixing nozzle. The air was at ambient temperature. The blower can deliver 1,8 kg/s of air at ideal conditions, but to get the correct flow ratio a piece of shade cloth was put in the inlet of the blower to lower the flow rate to between 0,45 to 0,5 kg/s.

4.2.3 Fans

The same fans used during the hot tests were used during the cold tests. For the cold tests a butterfly valve was fitted to the fans to make it possible to control the flow rate from the fans. For each number of fans switched on, the valve was set at 0% closed, 30% closed and 50% closed. This made it possible to have more than just four different flow rates from the set of fans.

4.2.4 Instrumentation

For the cold tests the following instrumentation was used:

Table 2: Instrumentation for cold tests

Channel	Parameter	Sensor	Range	Std Dev
1	Thrust	Strain gauge load cell	500 N	6,75 N
2	Flow from fans	Intake + differential pressure transducer	5 kPa	4,6 Pa
3	Flow from blower	Bellmouth + differential pressure transducer	1,2 kPa	1,79 Pa
4	Flow to thruster	Anubar + differential pressure transducer	5 kPa	3,85 Pa
5	Static pressure of ambient air at inlet of model	Static probe + Scani Valve	5 kPa	4,93 Pa
6	Static pressure of ambient air around mixing nozzle	Pressure ring + Scani Valve	5 kPa	4,93 Pa
7	Static pressure of blower air at exit of mixing nozzle	Static port + Scani Valve	5 kPa	4,93 Pa
8	Static pressure of air at thruster	Static probe + Scani Valve	5 kPa	4,93 Pa

All the above instrumentation was connected to a Hewlett Packard data acquisition system. This system makes use of a HP3456A data acquisition

control unit and a HP3497A digital volt meter(DVM).The data acquisition system is connected to HP9000 personal computer. The software (written in HP BASIC) used for these tests was modified from software already written for the computer and data acquisition system. The data acquisition system can read upto 40 analogue channels. The number of readings taken of each channel can be set by the software on the computer. The DVM automatically calculates the average for each channel and sends the value to the computer. The computer then applies the relevant calibration equation to each data channel and saves the values in the computer memory. After each test the data is saved onto a 3,5 inch disc.

To make it possible to process the data further on an IBM compatible PC, the data is converted from an ASCII- file (as saved by the HP computer) to a TEXT file (that can be read by the IBM compatible) by making use of a HP-VECTRA. The HP-VECTRA can run both the HP-BASIC and DOS operating systems.

4.3 Dual flow

The dual flow system was tested on the cold test rig to determine the effect of the change in the area ratio A_a/A_b would have on the static pressure of the gasses in the tail boom. From the comparison of the hot and cold tests on the single flow system it was seen that density does not have any effect on the performance coefficients. It was therefore decided to tests the dual flow system only on the cold tests rig.

4.3.1 Model

The model for the dual flow system tests consisted of the same mixing nozzle that was used for both the previous hot and cold tests. The inner tube was extended to the same length as the outer tube of the single flow system. The

inlet was expanded to a diameter of 300mm for connections to the concertina pipe. The mixing nozzle was sealed inside the inner tube. The outer tube was not used during these tests. The same thruster as used in the hot and cold tests was used in these tests. The thruster was bolted to the inner tube. A diagrammatic arrangement of the dual flow test rig is presented in figure 15:

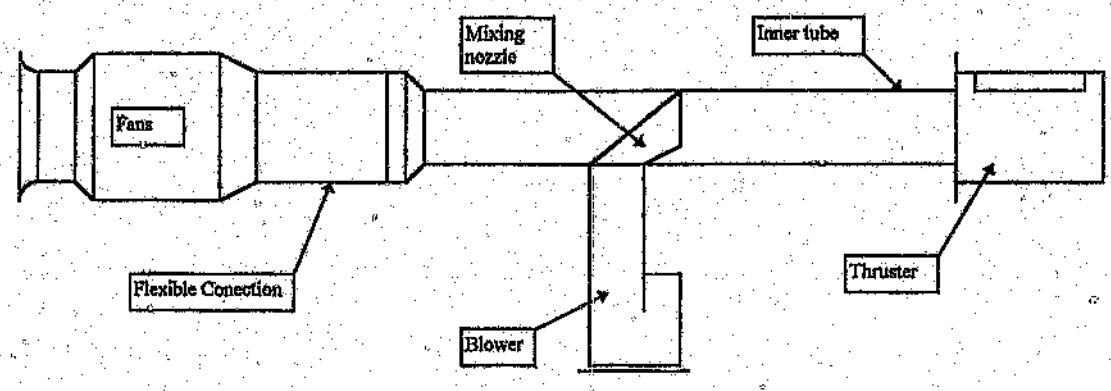


Figure 15: Diagrammatic arrangement of Dual flow test rig

4.3.2 Fans, Blower

The same equipment used for the cold tests was used for the dual flow tests.

4.3.3 Instrumentation

For the dual flow tests the following instrumentation was used.

Table 3: Instrumentation for dual flow tests

Channel	Parameter	Sensor	Range	Std Dev
1	Thrust	Strain gauge load cell	500 N	6,75 N
2	Flow from fans	Intake + differential pressure transducer	5 kPa	4,6 Pa

3	Flow from blower	Bellmouth + differential pressure transducer	1,2 kPa	1,79 Pa
4	Static pressure of ambient air at inlet of model	Static probe + Scani Valve	5 kPa	4,93 Pa
5	Static pressure of ambient air around mixing nozzle	Pressure ring + Scani Valve	5 kPa	4,93 Pa
6	Static pressure of blower air at exit of mixing nozzle	Static port + Scani Valve	5 kPa	4,93 Pa
7	Static pressure of air at thruster	Static probe + Scani Valve	5 kPa	4,93 Pa

The flow to the thruster was calculated by adding the flows from the fans and the blower. The same data acquisition system used for the single flow cold tests were used for the dual flow tests.

5 Test Procedures

5.1 Hot tests

The pressure transducers and load cell were first calibrated. The calibrations of equipment used for the hot tests are listed in appendix A

For the hot tests both the number of fans running and the flow rate through the burner were varied. The burner was first started and allowed to stabilise at a temperature of 450°C and a flow rate of 0,3 kg/s. The fans were then switched on (2,3 or 4). The flow rate through the burner was then set at four points between 0,3 kg/s and 1,1 kg/s. Ten readings were taken and averaged of each channel for each of these points.

Results from the hot tests appear in appendix C (See Table C1 to C3). The results for these tests are presented in three different tables. Each table represent a test with a different number of fans switched on, in this case, 4, 3 and 2 fans running. Each table then has three or four columns of data. These three or four columns (Point 1,2,3 etc.) represent the various flow rates through the burner for each of the tests. The fixed dimensions of the model appear at the bottom of each of the tables.

5.2 Cold tests

Different pressure transducers than those used in the hot tests were used in the cold tests. The calibration of the pressure transducers used for the cold tests are also listed in appendix A.

The pressures read by the static probes, as well as the flow rate measured by the anubar was also calibrated using a pitot tube. The calibration for these equipment also appear in appendix A

For the cold tests the flow rate through the blower was kept constant. The number of fans switched on and valve setting was varied to vary the flow ratio between the fan flow and the engine flow. The following settings were used:

No. of fans	Valve setting (% closed)
4	0
4	30
4	50
3	0
3	30
3	50
2	0
2	30
2	50

Fifty readings were taken and averaged for each channel for each of these settings. The results for the cold tests appear in appendix C (See Tables C4 to C6). The results for these tests are also presented in three different tables. As with the hot tests, each of these tables represent a different number of fans that are switched on. Each of the three columns (Point 1,2 & 3) in each of the tables represent the various settings of the valve that was used to choke the flow from the fan. The same fixed dimensions, as with the hot tests also appear at the bottom of these tables.

5.3 Dual flow tests

For the dual flow tests the flow through the blower was kept constant. The outlet area of the thruster was varied. For each of the four outlet areas of the thruster the number of fans was varied from four to one. For each fan setting the valve was set at 0% closed and 50% closed. The results of the dual flow tests appear in appendix C (See Tables C7 to C10). The data is devided into 4 tables. Each tables is for a specific thruster area ratio. The columns in each of these tables represent the various fan and valve settings, from Point 1 which is 4 fans on and valve fully open to Point 8 which is 1 fan on and the valve 50% closed.

The set-up as used for the dual tests was also used to measure the entrainment of the mixing nozzle. Entrainment is the flow of secondary air that is caused by the flow of air from the mixing nozzle. The jet effect of the air exhausting from the mixing nozzle draws the secondary flow into the mixing pipe. The entrainment ratio is the ratio of secondary air mass flow that is entrained devided by the mass flow from the nozzle (G_s/G_e). A diagrammatic arrangement of the model for measuring the entrainment appears in figure 16.

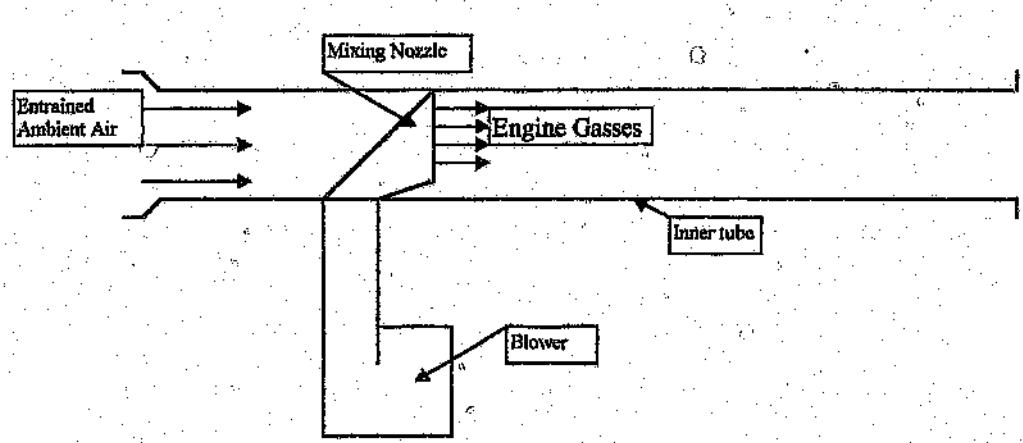


Figure 16: Diagrammatic arrangement of set-up to measure entrainment

The entrainment was measured by removing the fans and the thruster from the model. The blower was then set at various flow rates by varying the number of pieces of shade cloth in the inlet. The flow through the blower was then measured with the bellmouth intake, and the secondary flow was measured with a Pitot tube. The Pitot tube was traversed across three diameters and readings were taken at the following point along each diameter [15]:

Point 1: 0,032D
Point 2: 0,135D
Point 3: 0,321D
Point 4: 0,679D
Point 5: 0,865D
Point 6: 0,968D

where D is the diameter of the tube.

The readings from the three diameters were averaged to obtain the secondary flow. The results of the entrainment tests appear in appendix C.

6 Results and Discussion

6.1 Hot and Cold tests

6.1.1 Mass flow

The following mass flows are required to analyse the performance of CIRSTEL:

1. Flow from the burner (primary flow) - (Ge)
2. Flow from the fans (secondary flow) - (Ga + Gcctb)
3. Flow to the thruster - (Gf)
4. Flow to the circulation control slots (Gcctb)

For both the hot and cold tests, slits were used to allow air to flow to atmosphere as opposed to jet slots. This had the advantage that no thrust was developed, by the air flowing through the slits, that would effect the thrust measured to the thruster.

For the hot tests it was found the readings from the anubar in the thruster were not accurate. Due to the heat of the exhaust gasses, it was not possible to calibrate the anubar. The following equation was used to calculate the flow tc the thruster:

$$K_G = \frac{\dot{G}_{thr}}{(A \rho T)^{0.5}_{thr}} \qquad 6.1$$

with Kg = 0,8869 and a standard deviation of 0,0303 for the tests given in reference 16. The flow to the CC-slots was calculated from the difference of the air supplied by the fans and burner/blower and the flow through the thruster.

6.1.2 Thrust

Using the conservation of linear momentum across the thruster (see figure 17):

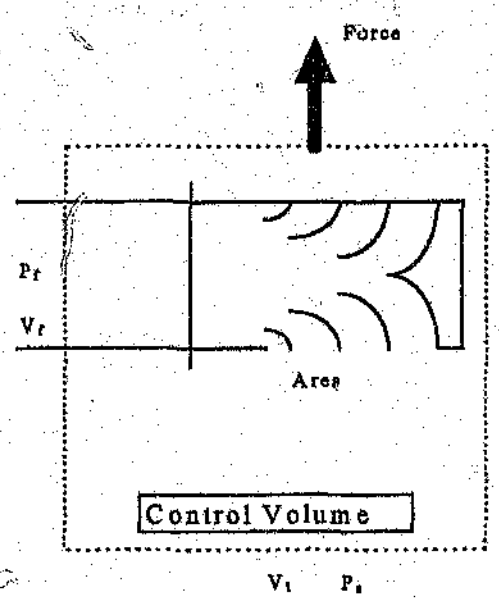


Figure 17: Control Volume across thruster

gives:

$$\Sigma F = G_f(V_f - V_t) + A_t(P_f - P_a) \qquad 6.2$$

assuming $V_t = 0$, equation 6.2 can be given as:

$$T = K_T(AP_t)_{thr} \qquad 6.3$$

where P_t is the total pressure at the entrance to the thruster and K_t is a constar to include unknown factors such as velocity components in the tail boom, non-uniform flow and expansion of the wake. (See reference 16)

The data obtained from the hot and cold tests were correlated using a least squares method to determine whether it could also be represented using equation (6.3). The data and linear fit appear in figure 18.

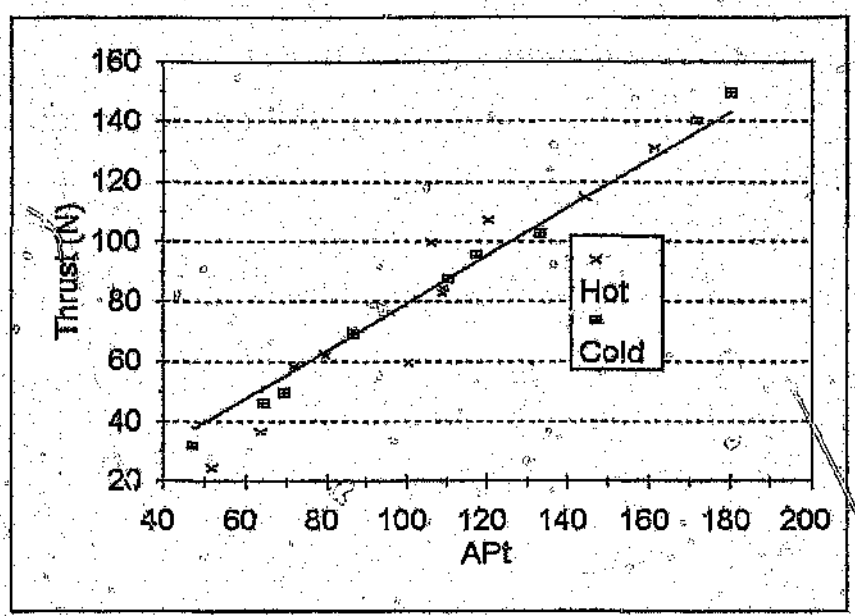


Figure 18: Variation of Thruster thrust with $(A P_t)_{thr}$

For these tests K_t = 0,794 with a correlation coefficient of 0.942. This value of K_t for the CIRSTEL tests is lower than the 1,060 obtained for the cold tests [16]. The CIRSTEL tests show a decrease of 25% in the value of K_t. From tests conducted at the University of the Witwatersrand it is now known that K_t is a function of the area ratio (A_T/A_b) of the thruster [9]. The area ratio for the tests conducted at the University of the Witwatersrand the area ratio was in the region of 0,2 to 0,4. For the tests carried out in this research program the area ratio was 1,1. This large variation in the area ratio would explain the variation of the value of K_t. The combined hot and cold results prove that it can not be temperature effects that cause this variation of K_t.

6.1.3 Power

6.1.3.1 Thruster

From the energy equation the power of the air supplied to the thruster can be given by:

$$P = \rho A V^3 \qquad 6.4$$

From Bernoulli's equation:

$$V = (2P_t/\rho f)^{0.5} \qquad 6.5$$

and from equation 6.3:

$$P_t = k(T/A) \qquad 6.6$$

Using equations 6.5 and 6.6 in equation 6.4 gives the following equation for predicting the power of the air supplied to thruster:

$$P = K_p \frac{T^{3/2}}{(A\rho)^{0.5}_{thr}} \qquad (6.7)$$

where K_p is a constant to include such effects as energy losses due to friction, a variation of the cross section of the jet leaving the thruster and the fan efficiency. (See reference 16)

The power of the air immediately upstream of the entrance to the thruster was calculated and then plotted against the T^3/2/(Aρ)^0.5 to determine whether equation (6.7) can be used when the air was hot. The data as well as the linear fit to the data appears in figure 19.

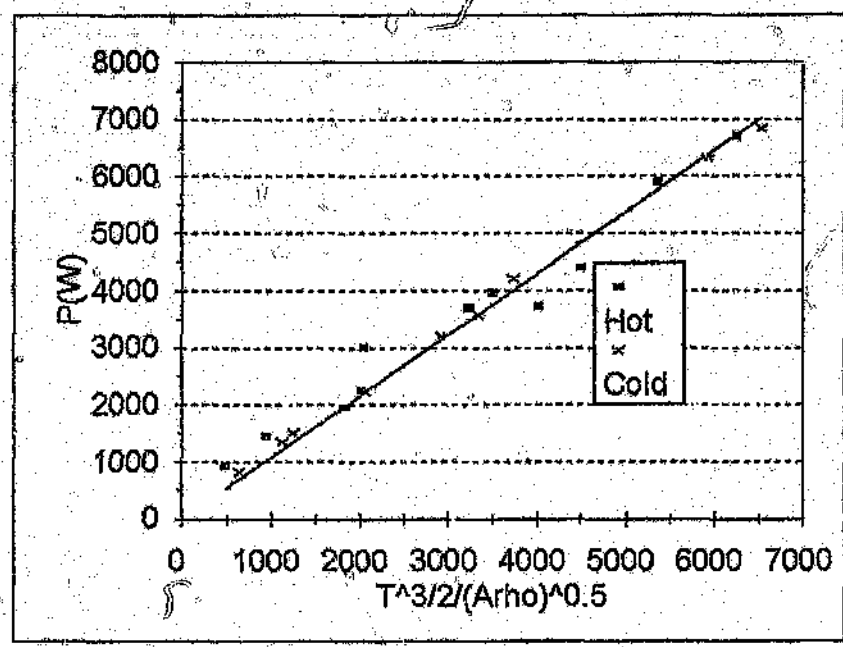


Figure 19: Variation of Thruster Power with $T^{3/2}/(A\rho)_{thr}^{0.5}$

For the linear fit it was found that K_p = 1,075 (with correlation coefficient of 0,989).This value is higher than the value of 0,822 obtained for the tests in [16]. From the correlation of the hot and cold tests it is clear that density has no effect on the value of K_p. This deference between the value of K_p obtained in [16] and obtained in these tests is due to the fact that K_p is a function of the area ratio of the thruster [9].

6.1.3.2 Fan

The power supplied to the thruster should be the sum of the power delivered by the fans and the nozzle (minus of course losses). Due to the different velocities of the two air streams (from fans and from nozzle) and the consequent shear stresses between the two air streams it is impossible to determine in a simple manner how the energy to the thruster is constituted. To obtain an indication of the power required from the fan at various flow ratios an equivalent power factor K_{pfan} was calculated using:

$$K_{Pfan} = \frac{P_{fan}(A\rho)^{1/2}}{T^{3/2}} \qquad 6.8$$

In the above equation 6.8, the thrust is the total thrust developed, while the power is the power attributed to the fans only. The resulting variation of K_{pfan} with velocity ratio is given in figure 20.

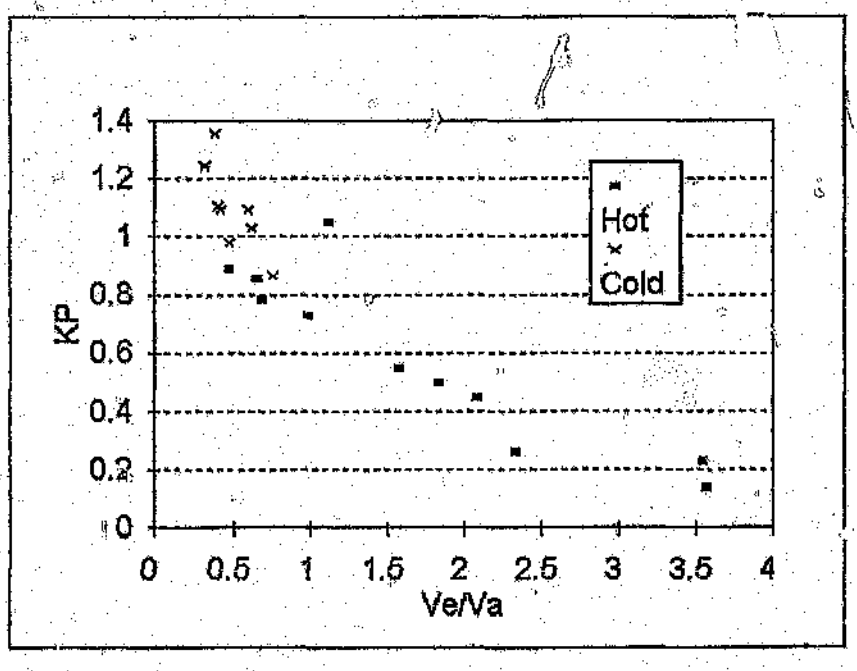


Figure 20: Variation of K_{pfan} with Velocity ratio

As shown in figure 20 the fan power is reduced significantly by the jet action of the hot gases from the mixing nozzle. As shown above the value of K_p for the thruster alone is 1,075 and would be higher if the losses over the mixing nozzle and along the tail boom were taken into account. The flow ratio for a CIRSTEL anti-torque system would be in the order of 0,9. From this it could be expected that the value of K_p would be in the region of 0,7. This means that the power requirements of the fans would be reduced by approximately 30%. This 30% of the power would then be supplied by the engine exhaust gasses. The effect of this on the engine performance needs to studied.

6.1.4 Static pressure

6.1.4.1 Fan Air

The static pressure of the air supplied by the fans from a point upstream of the mixing nozzle to the inlet of the thruster should be quantified to ensure that the static pressure of the air supplied to the circulation control slots will be sufficient to allow a torque to be developed by the tail boom.

The drop in static pressure of the fan air from the fan exhaust to the inlet of the thruster will depend on a number of factors. These include the change in total energy of the air per unit mass due to mixing, turbulent shear stresses and losses due to flow expansions. Reference [13] discusses the difficulties of predicting the performance of mixing nozzles.

A momentum balance (for the flow from the fan) across the tail boom from the mixing nozzle exit to the thruster entrance, ignoring shear stresses and flow across the control volume (See figure 21):

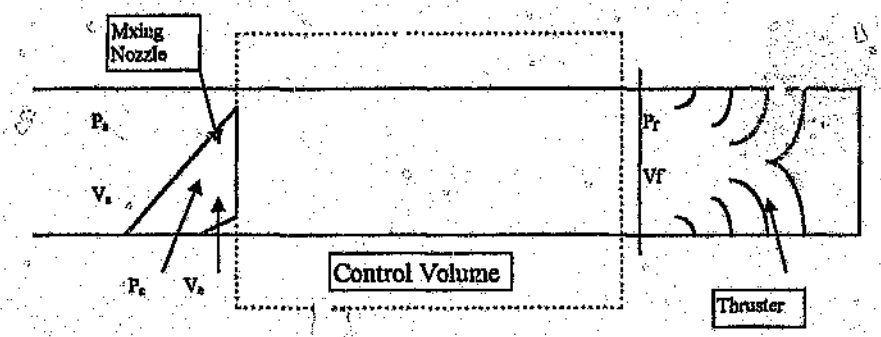


Figure 21: Control Volume across tail boom

gives:

$$\Sigma F = \int V(\rho V dA) \qquad 6.9$$

From equation 6.9:

$$P_a - P_f = \rho_f V_f^2 - \rho_a V_a^2 \qquad 6.10$$

For the case of no flow from the engine and no losses across the mixing nozzle and in the tail boom, equation 6.10 can be written as:

$$\frac{P_a - P_f}{\rho_f V_f^2 - \rho_a V_a^2} = 1 \qquad 6.11$$

A change in energy per unit mass of air for a given flow condition will manifest itself as a change in static pressure at the entrance to the thruster. This change in energy will be a function of the losses on the wall of the tail boom and also the mass flow ratio. To determine whether it is possible to express the pressure

loss in terms of the mass flow ratio only, equation 6.11 is written as follows: (see references [3] and [17]):

$$\frac{P_a - P_f}{\rho_f V_f^2 - \rho_a V_a^2} = f\left(\frac{G_e}{G_a}\right) \qquad 9.12$$

where f is a universal function of the mass flow ratio. To determine whether such a universal function for the geometry of the CIRSTEL exists, the LHS of equation 6.12 was plotted against the mass flow ratio in figure 22.

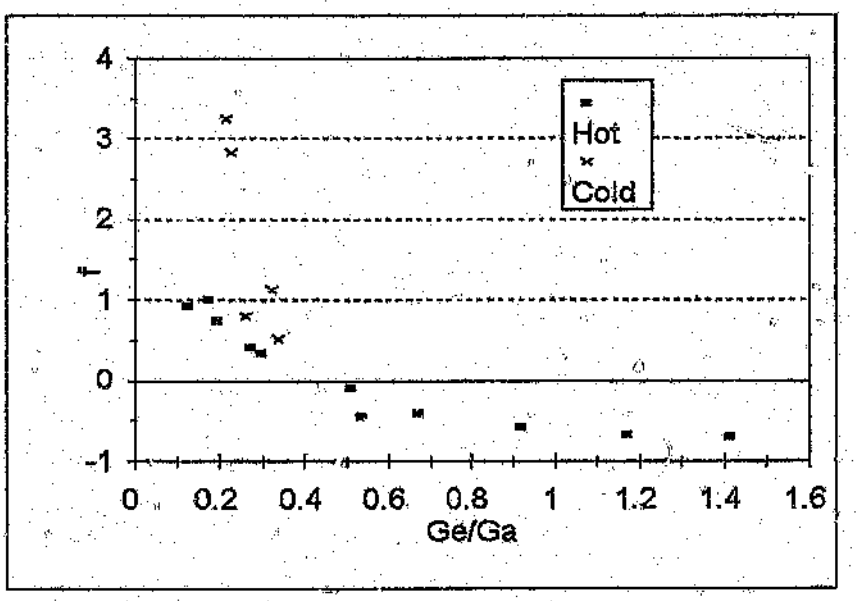


Figure 22: Variation of function f with mass flow ratio

It is clear from figure 22 that f is, to good approximation, a function of the mass flow ratio for the geometry tested. At a flow ratio of 0 (no flow from the engine) and no losses across the nozzle the value of f should be unity. Due to losses in the tail boom the value of f is greater than unity for a flow ratio of 0. As the flow from the engine increases the value of f drops. This is caused by the fact that as the flow from the engine increases the internal energy of the air in the tail boom increases(P_f increases). The static pressure at the inlet to the thruster will also

increase as the flow through the thruster increases. It can therefore be expected that the value of f will decrease as the flow ratio increases. For a flow ratio of greater than 0,5 the value of f becomes negative. The static pressure of the air at the entrance to the thruster will therefore be greater than the static pressure of the air upstream of the nozzle.

For the CIRSTEL system the mass flow ratio will probably be in the region of 0,25. The value of f will therefore be approximately 0,5. From the figure 22 it will therefore be very easy to determine the value of f, and from that the difference in static pressure between the points of interest, for any flow condition.

6.1.4.2 Engine exhaust gases

The static pressure of the gases at the exit of the mixing nozzle will be the back pressure that is imposed on the engine exhaust gases. It will be necessary to determine this pressure and how it will vary for all flow conditions.

Using the momentum balance from across the nozzle exit to the thruster entrance (as used in 6.1.4.1, see figure 21)

$$P_e - P_f = \rho_f V_f^2 - \rho_e V_e^2 \qquad 6.13$$

produces the following dimensionless relationship(see references[3] and [17]):

$$\frac{P_e - P_f}{\rho_f V_f^2 - \rho_e V_e^2} = g\left(\frac{G_e}{G_a}\right) \qquad 6.14$$

where g is a universal function of the mass flow ratio. To determine whether such a universal function for the geometry of the CIRSTEL tail boom exists, the LHS of equation 6.14 is plotted against the mass flow ratio in figure 23:

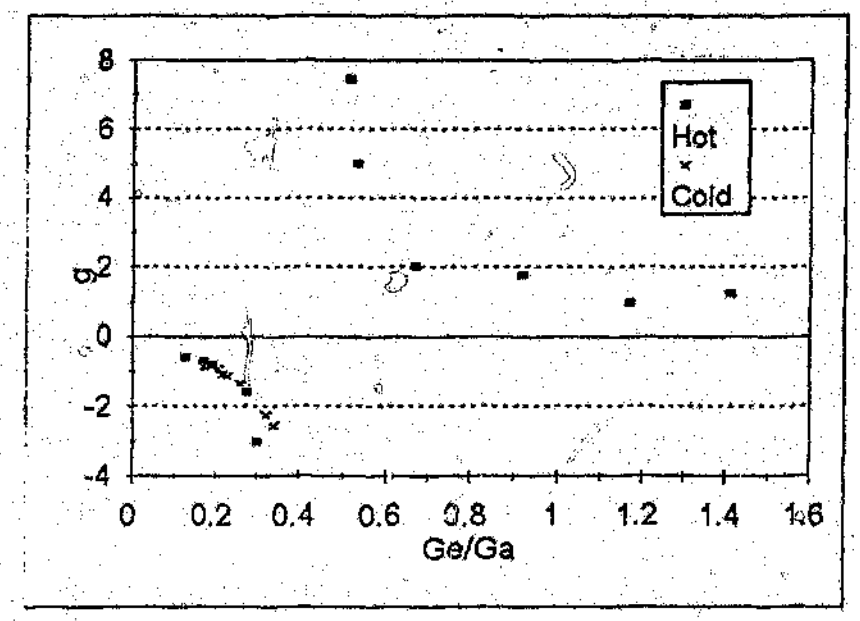


Figure 23: Variation of function g with mass flow ratio

From figure 23 it can be seen that g is in fact a universal function of the mass flow rate. At a mass flow ratio of 0 the static pressure at the outlet to the nozzle should be the same as the static pressure at the inlet to the thruster. As the flow from the engine increases the value of g will decrease due to the jet effect of the fan air on the flow from the engine. This decrease will continue until the flow from the engine starts developing a jet effect on the flow from the fan. When this occurs the static pressure of the gasses in the nozzle will become greater than the static pressure in the thruster and g will change from negative to positive. This transition will take place when the denominator of the dimentionless group in equation 6.14 becomes zero, therefore when $\rho_e V_e^2 = \rho_f V_f^2$. Using the density ratio $\rho_e/\rho_f = 0.9$ and the area

ratio A_e / A_t of 0,35 the approximate transition point is at the mass flow ratio of 0,5.

As the mass flow ratio increases to infinity (flow from fans become zero) the value of g tends to 1. This means that the flow from the engine is merely expanding from one area to the other, which can easily be solved with Bernoulli's equation.

As it is expected that the CIRSTEL concept will operate at a mass flow ratio of 0,25 it is clear from figure 23 that this is in the region where the flow from the engine is dominated by the flow from the fans. The static pressure of the flow from the engine will therefore increase from the nozzle exit to the thruster inlet. As the absolute value of g is below unity , the increase in pressure will not be significant.

6.1.5 Temperature

6.1.5.1 Thruster Jet

If is assumed that all energy losses from the system is negligible, an energy balance can be written as follows:

$$G_t\left(C_{Pt}T_t + \frac{V_t^2}{2}\right) = G_a\left(C_{Pa}T_a + \frac{V_a^2}{2}\right) + G_e\left(C_{Pe}T_e + \frac{V_{ef}^2}{2}\right) \qquad 6.15$$

Cp is given by [18]

$$C_p = 1.0036 + 0.0702x10^{-3}T + 0.1715x10^{-6}T^2 - 0.0702x10^{-9}T^3 \qquad 6.16$$

For the tests carried out the kinetic energy was less than 0,5% than the total internal energy of the gas. On averaging C_{Pf}, the temperature of the gasses exiting the thruster can thus be approximated by re-writing equation 6.16. (see reference [17]) :

$$T_f = \frac{C_{pe} T_e \left(\frac{G_e}{G_a}\right) + C_{pa} T_a}{C_{pe} \left(\frac{G_e}{G_a}\right) + C_{pa}} \qquad 6.17$$

As variation of Cp will be very small for the temperatures considered in this case, it is clear that the temperature of the jet is only a function of the mass flow ratio, the temperature of the fan air and the temperature of the gasses exiting the nozzle. The variation of equation 6.17 with the measured temperatures is plotted against the mass flow ratio in figure 24.

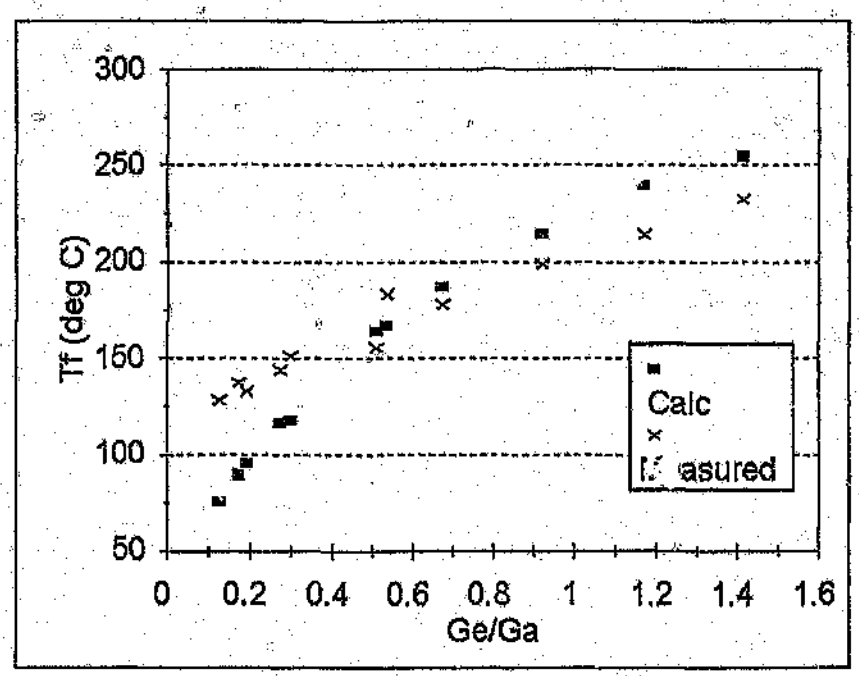


Figure 24: Variation of T_f with mass flow ratio

It is clear from figure 24 that the measured temperature is lower than the calculated temperature at high mass flow ratios. This shows that good mixing took place and that the loss of thermal energy through the skin of the tail boom is not insignificant. It is likely that the temperature of the thruster jet will be reduced further if the flow could be brought up to the scale values.

6.1.5.2 Tail boom skin

Any large variation of the temperature of the tail boom skin with ambient temperature must be avoided because this will give a significant signature to infra-red guided missiles. The difference of the temperature of the surface of the tail boom with ambient temperature is plotted against mass flow ratio in figure 25.

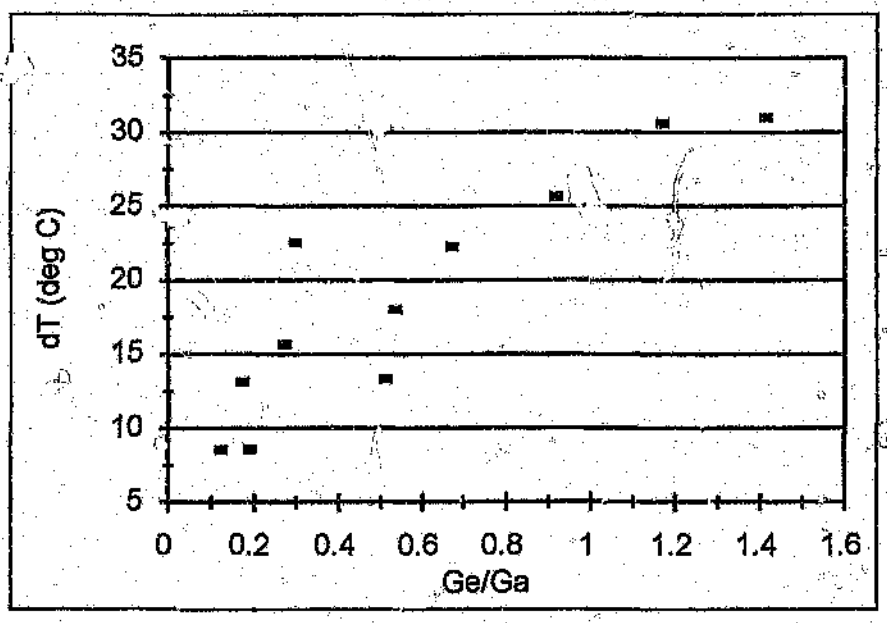


Figure 25: Variation of Tail Boom Surface Temperature with mass flow ratio

The temperature difference seems to increase with an increase in mass flow ratio. This is to be expected as an increase in mass flow ratio is in fact an increase in engine mass flow rate. It should be noted that the flow rate through

the circulation slots was lower than calculated and the temperature of the surface of the tail boom can be brought down further by increasing the flow through the circulation slots to the correct value. The effect of the down wash from the main rotor is also not taken into consideration in this analysis. This would bring down the temperature difference even further.

A detail study is however required to ensure that no hot spots occur anywhere on the model. The thruster will be especially prone to hot spots as the flow in halve the volume of the thruster is standing still, and therefore increases the heat transfer to the surface.

6.2 Dual Flow Tests

6.2.1 Entrainment

The variation of entrainment ratio (Ga/Ge) versus blower volume flow rate is plotted in figure 26.

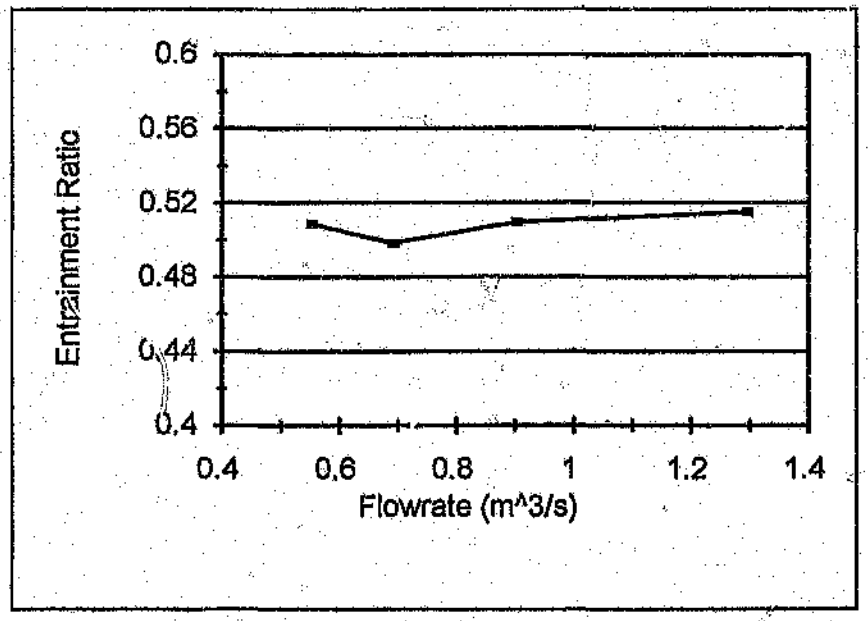


Figure 26: Variation of Entrainment ratio with blower flow

From figure 26 it can be seen that the average entrainment ratio is 0,5. This low value of entrainment can be ascribed to the asymmetrical shape of the nozzle as well as the non-ideal area ratio of the dual flow system [19]. Further tests with varying area ratios are necessary to obtain the optimum area ratio.

6.2.2 Mass flow

Only the air flows from the fans and blower were measured for the dual flow tests. The flow to the thruster was calculated by adding the flows from the blower and the fans. For the dual flow tests the secondary flow is therefore the total flow from the fans.

6.2.3 Static Pressure

6.2.3.1 Fan air

To predict the static pressure drop of fan air, the same function f (equation 6.12) as used in 6.1.4.1, is plotted is against the velocity ratio in figure 27. Because the temperatures of the two air streams are equal it is not necessary to plot the function against the mass flow ratio. The legends denote the thruster outlet area ratio.

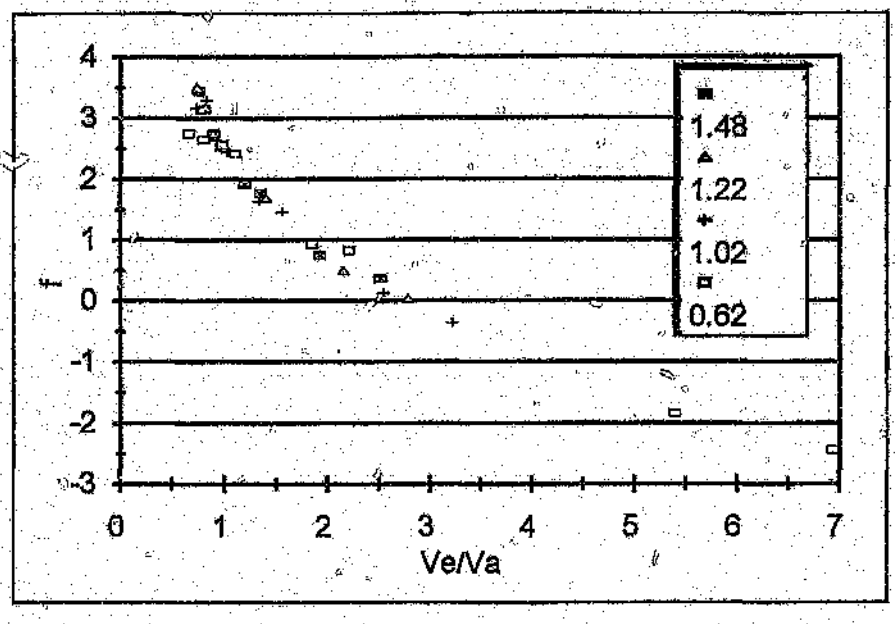


Figure 27: Variation of function f with velocity ratio for dual flow system

As can be seen from figure 27 the static pressure drop of the fan air is a function of the velocity ratio. The function also shows the same characteristics as that for the single flow system. The transition point (from pressure drop to pressure rise) has shifted to a higher value of velocity ratio. This shift is possibly due to the change in the area ratio A_e/A_b. It is clear from figure 27 that the thruster outlet area does not affect the function f.

6.2.3.2 Engine exhaust air

Using the same function g as used in 6.1.4.2 (equation 6.14) but also plotting it against the velocity ratio, produces the following graph (the legends denote the thruster outlet area):

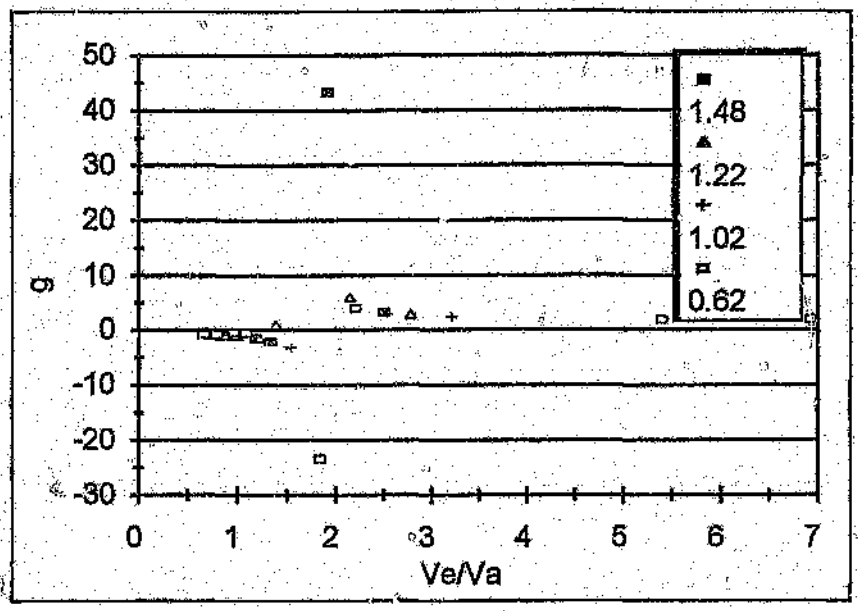


Figure 28: Variation of function g with velocity ratio for dual flow system

As can be seen from figure 28, $g(V_e/V_a)$ represents a function of the static pressure drop of the engine exhaust gasses. The graph for the dual flow system shows the same characteristics as the graph for the single flow systems. Also with this function g, the transition point has shifted to a higher value of the velocity ratio. As with the fan air this shift is possibly due to the change in the area ratio A_e/A_b. It is also possible that the shift is due the fact that no air is being exhausted through the circulation control slots. It is clear from figure 28 that the outlet area of the thruster does not affect the function g.

7 Conclusions

7.1 Thruster

It is possible to characterise the performance of a thruster with a fixed geometry fitted to the CIRSTEL model by means of the values K_p and K_t.

The value obtained for K_t in these tests is approximately 25% lower than the value obtained for tests carried out at the University of the Witwatersrand. The value obtained for K_p in these tests is approximately 25% higher than the value obtained for the tests done at the University of the Witwatersrand. These variations are due to fact that K_p and K_t are dependent on the area ratio of the thruster [9].

From the combined correlation of the Hot and Cold tests it is clear that K_p and K_t are not affected by temperature.

7.2 Fan Power

The power required from the fans are significantly reduced by the introduction of the hot engine gasses into the tail boom. This reduction in power can be described by the value of K_{pfan}, which is a function of the velocity ratio (V_e/V_a) of the engine gasses and fan air. As can be seen from figure 20, the value of K_{pfan} is reduced from a value of 1,075 for the thruster alone to approximately 0,7, at a velocity ratio of 0,9. This equates to a 30% reduction in the power required from the fans due to he introduction of the hot engine gasses into the tail boom. The effect of this on the performance on the engine will of course have to be studied.

7.3 Static Pressure

7.3.1 Fan air

7.3.1.1 Single flow system

The static pressure drop of the air from the fans can be described by the function f. This function f is a function of the mass flow ratio (G_e/G_s). The flow can be devided into to regimes. At a mass flow ratio below 0,5 the static pressure of the fan air drops from the around the mixing nozzle to the entrance of the thruster. This drop in static pressure decreases as the mass flow ratio increases from 0 to 0,5. This is caused by the increase in internal energy due to the introduction of the hot engine gasses into the tail boom. At a mass flow ratio of above 0,5 the static pressure of the fan air rises (pressure drop becomes negative) from around the mixing nozzle to the entrance of the thruster.

This means that if it was possible to vary the mass flow ratio, it would be possible to control the static pressure of the fan air. The mass flow ratio for the CIRSTEL concept is however set at 0,25. The value of the function f at this mass flow ratio is below one, therefore the drop in static pressure will not be significant.

7.3.1.2 Dual flow system

The dual flow system shows the same characteristics as the single flow system. The transition point of pressure drops to pressure rise has however shifted for the dual flow system. This is possibly due the change in the area ratio A_e/A_b and/or the fact that no air is exhausting through circulation control slots.

The flow is devided into two regimes. Below a velocity ratio of below 2, the static pressure drops. At a velocity ratio of above 2, the static pressure of the fan air rises. From the fact that the data for these tests (with varying thruster outlet areas) were plotted on the same graph it is clear the outlet area of the thruster does not affect this function.

7.3.2 Engine exhaust gasses

7.3.2.1 Single flow system

The static pressure drop of the gasses from the engine can be described by the function g. This function g is a function of the mass flow ratio. As with the fan air, the flow can be devided into two regimes. At a mass flow ratio from 0 to 0,5 the static pressure of the engine exhaust gasses rises from the exit of the mixing nozzle to the entrance of the thruster. This is due to he jet effect that the flow from the fan has on the flow from the engine. At a flow ratio of just above 0,5 the static pressure drop of the engine gasses is very large and then decreases significantly as the flow ratio increases further. In this flow regime the flow from the engine now has a jet effect on the flow the fans.

This means again that, if the mass flow ratio could be varied, it would be possible to control the static pressure drop of the engine exhaust gasses. As the mass flow ratio for the CIRSTEL model is set at 0,25 it is clear that the absolute value of the function g is less than unity, and the pressure rise is therefore not very significant.

7.3.2.2 Dual flow system

Once again the dual flow system shows the same characteristics as the single flow system. The flow can also be devided into two regimes. At a velocity ratio of below 2, the static pressure of the engine gasses rises, and at a velocity ratio of above 2, the static pressure drops.

This shift in the transition point when compared to the single flow system can possibly be ascribed to the change in the area ratio A_e/A_b and/or the fact that no air is being exhausted through circulation control slots.

As with the function f, the data for the tests with varying thruster outlet area was plotted on the same graph and it is therefore clear that the outlet area of the thruster does not have any effect on the function g.

7.4 Temperature

7.4.1 Thruster Jet

The temperature of the air exiting the thruster can be approximated by equation 6.17. The temperature calculated with this equation is higher than the measured temperature. This is possibly due to energy transferred through to skin of the model. The variation at low mass flow ratios is possibly due to inaccuracies in the flow measurements.

The temperatures measured were in the region of 150 to 200 °C. This is a significant reduction from the 450 °C of the engine exhaust gasses. It must however be noted that the mass flow from the fan was lower than the scale value. This temperature could therefore be reduced even further is the correct value of flow from the fans could be obtained.

7.4.2 Tail boom skin

The variation of the temperature of the tail boom skin with the ambient temperature seems to vary with the mass flow ratio. This variation does not however take into consideration the flow from the main rotor that could significantly reduce this temperature difference.

The highest temperature of the tail boom skin measured was 54 °C. This temperature will be reduced if the effects of the downwash from the main rotor were also simulated. The flow from the circulation control slots was also lower than the scale value. This means that the temperature will be reduced even further if the flow through the circulation control slots is correct.

7.5 Entrainment

The average entrainment ratio of the mixing nozzle was measured at 0,5. This is quite low. It is possible due to the asymmetrical shape of the nozzle, of well as the area ratio: A_e/A_b. As it is likely that an increase in the entrainment ratio would mean a further reduction the power requirements of the fan, the area ratio and nozzle shape should be optimised to increase the entrainment ratio as much as possible.

8 Suggestions for further work

The tests conducted in this research program made it possible to obtain a overall base line for the design of CIRSTEL system. It is however still necessary to obtain more detailed information regarding the subjects discussed below to ensure that a clearer picture of the difference in performance between the single and dual flow systems is available.

8.1 Pressure

8.1.1 Static pressure drop

From the tests conducted in this study it is clear that the area ratio (A_a/A_b) has an effect on the drop in static pressure of both the ambient air from the fans and the hot engine gasses. Further tests, with more values of the ratio A_a/A_b, are required to determine a possible relationship between the area ratio (A_a/A_b) and the drop in static pressure of the two flows.

8.1.1 Dual flow Secondary flow

No tests were done to characterise the flow in the outer section of the dual flow system. Tests will have to be conducted to ensure that the pressure in the outer section is sufficient to produce the required torque from the circulation control.

8.2 Temperature

8.2.1 Single flow system

Although the temperature of the tail boom skin was measured during the hot tests on the single flow system, these tests do not include the effect of the down wash from the main rotor or the effect of forward flight of the helicopter. It is possible that the temperature of the tail boom skin could be further reduced if these effects are taken into consideration.

8.2.2 Dual flow system

The dual flow system has to be tested on the Hot Gas Test Facility to determine the temperature of the mixed air exhausting from the thruster. This temperature will be higher than the temperature for the single flow system, as less ambient air will be available for mixing with the hot exhaust gasses.

The temperature of the air in the outer section of the dual flow system will also have to be measured. The flow in the outer section will be lower than in the single flow system. It is therefore possible that the temperature of this air will be higher than for the single flow system. This would mean that the temperature of the tail boom skin for the dual flow system will be higher than for the single flow system. Tests will have to conducted to ensure that these temperatures are below the limits for infra-red detection.

8.3 Engine

The effect of the back pressure on the engine due to the exhaust gasses being ducted into the tail boom needs to be studied to ensure that the performance of the engine is not severely effected.

8.4 Diffuser-Thruster

The Diffuser-Thruster must also be tested as an option for the CIRSTEL option. The higher mass flow rate of ambient air will make the DT very feasible when the reduction of engine exhaust gas temperature is taken into consideration.

9 References

1 Prouty R **The Pros and Cons of the Fan-in-Fin**, Rotor and wing, November 1992

2 McClellan J **No Tail Rotor**, Flying, February 1991

3 Nurick A and Bouwer P **An Investigation of the Cooling of Engine gases through a Circulation Control Tail boom**, 20th European Rotorcraft Forum, Amsterdam, October 4 - 7, 1994

4 Logan A H **NOTAR** Veriflite, Vol. 28, No. 3, March/April 1982, pp20 - 23

5 JanakiRam R D and Currier J F **Noise Characteristics of Helicopters with the NOTAR™ Anti-Torque System**, Royal Aeronautical Society Conference: The Quiet Helicopter, London, 1992

6 Jonkers R J et al **Pre-Feasibility Study for the Development of a Helicopter Anti-Torque System in Combination with Engine Exhaust Infra-red Suppression**, April 1993

7 Nurick A **Performance of a Scaled Helicopter Circulation Controlled Tail Boom and Thruster Anti-Torque Facility** School of Mechanical Engineering Research Report No94, University of the Witwatersrand, October 1993

8 Nurick A, Rollemo G and Kaptein R **Preliminary Evaluation of a Diffuser-Thruster for use as a Helicopter Anti-Torque System** 19th European Rotorcraft Forum, Cernobbio (Como), Italy, September 14 -16, 1993

9 Nurick A **Unpublished Results**

10 Hanvey S A **No Tail Rotor (Circulation Control Tail Boom)**, 26th Annual Symposium of the Society of Experimental Test Pilots, 25 September 1982

11 Kelly H L and Wilson J C **Helicopter Anti-Torque System using Fuselage Strakes; Patent Aplication** US-PAT-APPL-SN-008895 Hamptom, VA, The Center, 1987

12 Nurick A and Groesbeek C **Experimental and Computational Invesigation of a Circulation Controlled Tail Boom** Paper B05, 18th European Rotorcraft Forum, Avignon, France, 15 - 18 September, 1992

13 Toulmay F, **Internal Aerodynamics of Infra-red Suppressors for Helicopter Engines**, 40th Annual national Forum of the American Helicopter Society, Arlington Virginia, May 16-18, 1984

14 Ashley S **Tomorrow's High-Tech Helicopter** Mechanical Engineering, June, 1991

15 Air flow, Operating Instructions 9004474-583, Pitot Static Tube

16 Nurick A **An Experimental Investigation of the Static Performance of Helicopter Thruster** School of Mechanical Engineering Research Report No.95, University of the Witwatersrand, March 1994

17 Bouwer P and Nurick A **An Experimental investigation of a 1/2 scale combined helicopter anti-torque and engine exhaust gas cooling model** Aerotek Report No. 95, March 1994

18 Kobe K A **Thermochemistry for the Petrochemical Industry Petrol Refiner.**, January 1949 - November 1949 - November 1954

19 Baumbach J and Bouwer P **Private Discussion**, July 1994

Appendix A
Calibration of Equipment

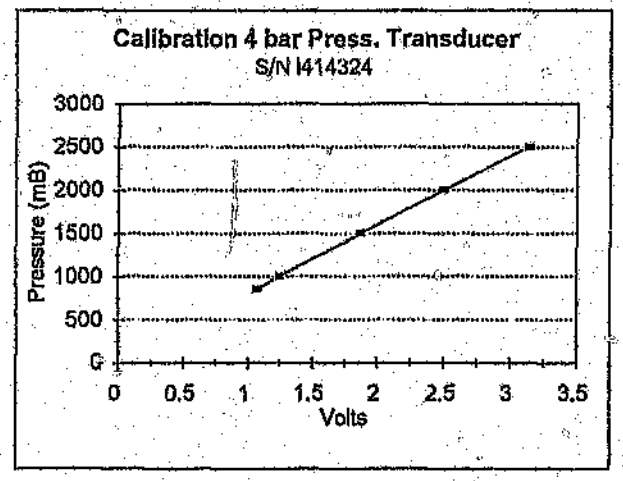
Calibration of 4 bar pressure transducer
S/N L414423
Test :Hot
Position: Ptotal - Primary Flow

Pressure mB	Volts
860.8	1.075
1000	1.249
1500	1.876
2000	2.5
2500	3.15

Regression Output:

Constant	12.4406
Std Err of Y Est	6.40554
R Squared	0.999935
No. of Observations	5
Degrees of Freedom	3

X Coefficient(s)	791.7357
Std Err of Coef.	3.696391

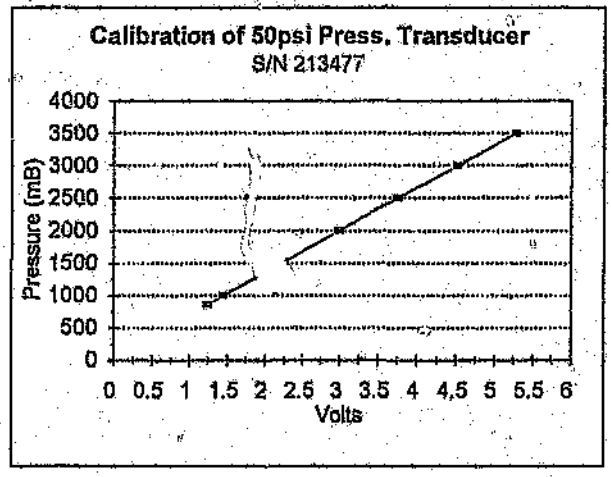


Calibration of 50 psi press. Transducer
S/N 213477
Test : Hot
Position: Ptotal - Thruster

Pressure mB	volts
861	1.245
1000	1.456
1500	2.223
2000	2.991
2500	3.758
3000	4.525
3500	5.289

Regression Output:

Constant	49.63853
Std Err of Y Est	0.800882
R Squared	0.999999
No. of Observations	7
Degrees of Freedom	5
X Coefficient(s)	652.1865
Std Err of Coef.	0.21273



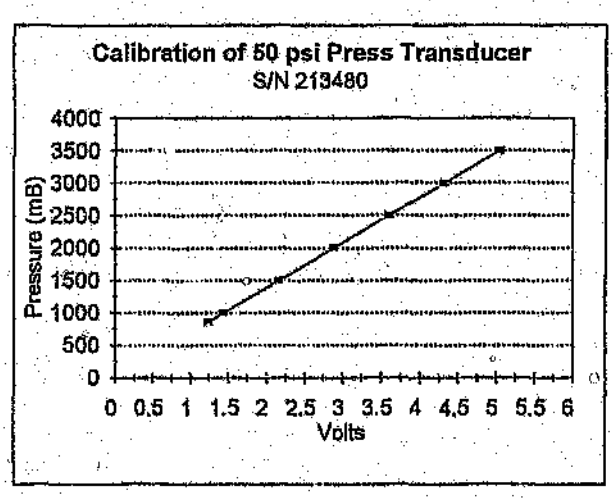
Calibration of 50 psi press. Transducer
S/N 213480
Test : Hot
Position: Pstatic - Primary Flow

Pressure mB	volts
861	1.246
1000	1.445
1500	2.164
2000	2.884
2500	3.604
3000	4.324
3500	5.043

Regression Output:

Constant	-4.19276
Std Err of Y Est	0.409028
R Squared	1
No. of Observations	7
Degrees of Freedom	5

X Coefficient(s)	694.6503
Std Err of Coef.	0.115753



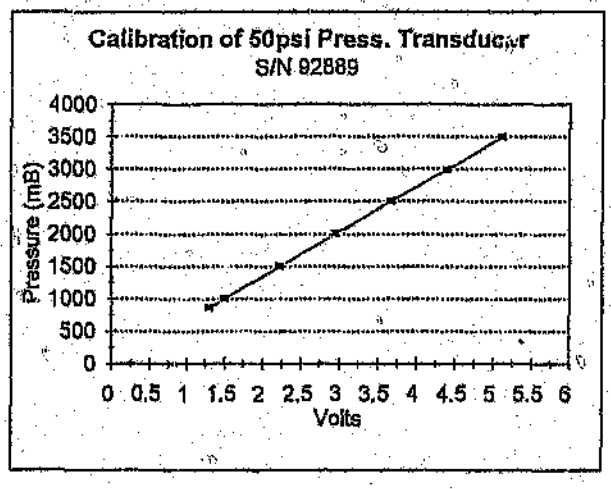
Calibration of 50 psi press. Transducer
S/N 92889
Test : Hot
Position: Pstatic Secondary Flow

Pressure mB	volts
861	1.304
1000	1.505
1500	2.23
2000	2.954
2500	3.678
3000	4.403
3500	5.128

Regression Output:

Constant	-38.8005
Std Err of Y Est	0.274105
R Squared	1
No. of Observations	7
Degrees of Freedom	5

X Coefficient(s)	690.152
Std Err of Coef.	0.077046



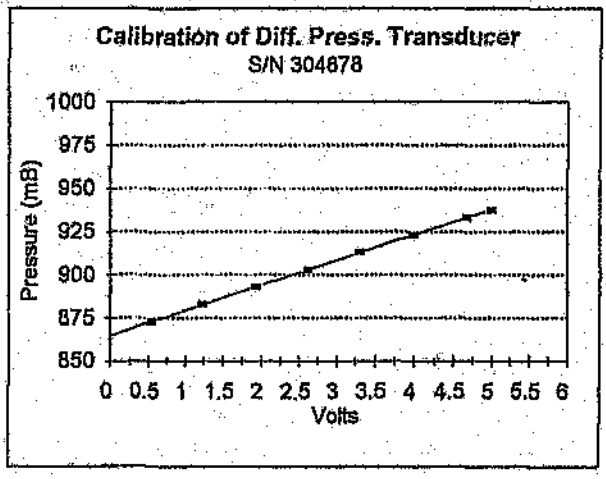
Calibration of 30" WC diff press. Transducer
S/N 304878
Test :Hot
Position: Delta P - Secondary Flow

Pressure mB	volts
862.9	-0.135
872.9	0.551
882.9	1.24
892.9	1.929
902.9	2.616
912.9	3.305
922.9	3.991
932.9	4.68
937.49	5.007

Regression Output:

Constant	864.8926
Std Err of Y Est	0.052137
R Squared	0.999997
No. of Observations	9
Degrees of Freedom	7

X Coefficient(s)	14.52106
Std Err of Coef.	0.010123



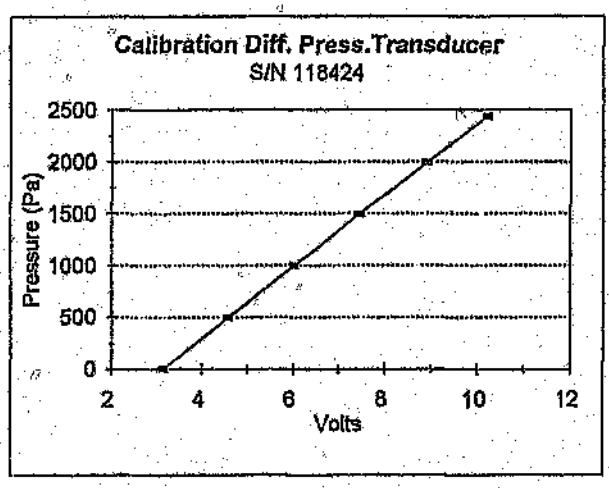
Calibration of 0.5 PSI diff press. Transducer
S/N 118424
Test : Hot
Position : Delta P, Thruster

Pressure Pa	Volts mV
0	3.145
497.1	4.59
996.3	6.0137
1493.95	7.4402
1992.4	8.8969
2442	10.22
1992.4	8.918
1493.95	7.465
996.1	6.0086
497.1	4.5677
0	3.1539

Regression Output:

Constant	-1085.4
Std Err of Y Est	4.719522
R Squared	0.999971
No. of Observations	11
Degrees of Freedom	9

X Coefficient(s)	345.6558
Std Err of Coef.	0.622655



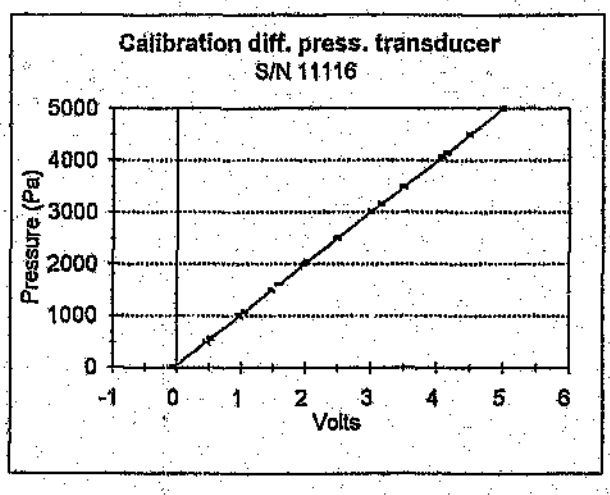
Calibration of 5kPa Diff Press. Transducer
S/N11116
Test : Cold
Position : Fan flow rate

Pressure Pa	Volts V
0	-0.03167
560	0.5333
1075	1.0597
1600	1.5847
2030	2.0233
2500	2.5012
3000	3
3500	3.5045
4080	4.0843
4500	4.501
5000	5.0076
4500	4.5024
4150	4.1548
3500	3.4976
3160	3.1554
2500	2.4911
2000	1.9874
1500	1.4865
1000	0.98158
500	0.47807
0	-0.0321

Regression Output:

Constant	26.60925
Std Err of Y Est	4.030438
R Squared	0.999994
No. of Observations	21
Degrees of Freedom	19

X Coefficient(s)	992.5803
Std Err of Coef.	0.572574



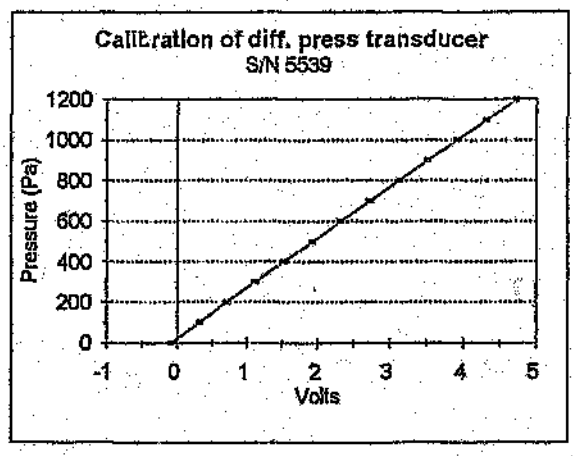
Calibration of diff. press transducer
S/N 5539
Test : Cold
Position : Blower flow rate

Pressure Pa	Volts V
0	-0.07576
104	0.3399
201	0.7117
301	1.1217
400	1.517
500	1.9202
600	2.3176
700	2.7178
800	3.1122
900	3.5236
1000	3.9196
1100	4.3212
1200	4.7215
1100	4.3289
1000	3.9185
900	3.5221
800	3.1268
700	2.7281
600	2.3182
500	1.9291
400	1.5245
300	1.1334
200	0.7348
100	0.3254
0	-0.0815

Regression Output:

Constant	19.34275
Std Err of Y Est	1.570573
R Squared	0.999983
No. of Observations	25
Degrees of Freedom	23

X Coefficient(s)	250.0592
Std Err of Coef.	0.217502



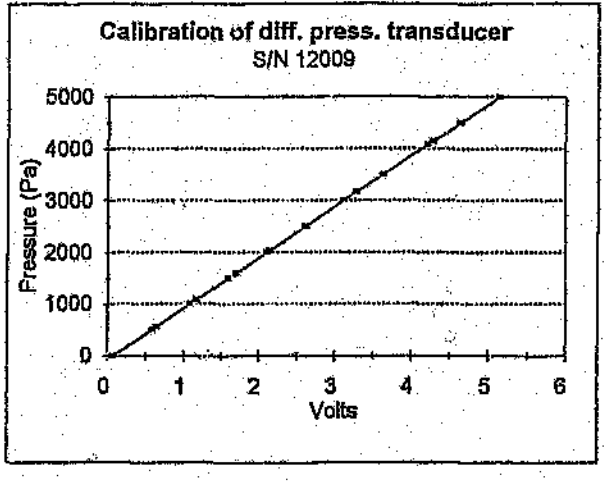
Calibration of diff. Press transducer
S/N 12009
Test : Cold
Position : Thruster flow rate

Pressure Pa	Volts V
0	0.07479
560	0.64112
1075	1.1718
1600	1.6942
2030	2.1368
2500	2.6152
3000	3.1175
3500	3.6254
4080	4.2097
4500	4.6294
5000	5.1423
4500	4.6295
4150	4.281
3500	3.6194
3160	3.2746
2500	2.606
2000	2.1009
1500	1.5982
1000	1.0916
500	0.58703
0	0.07973

Regression Output:

Constant	-77.7085
Std Err of Y Est	3.386501
R Squared	0.999996
No. of Observations	21
Degrees of Freedom	19

X Coefficient(s)	987.9211
Std Err of Coef.	0.478836



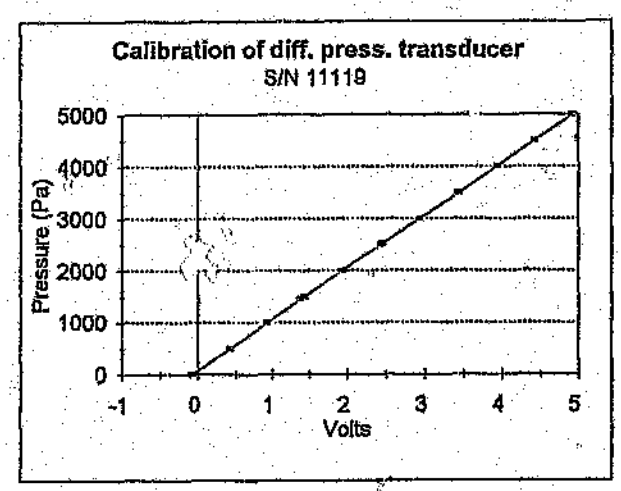
Calibration of diff. press. transducer
S/N 11119
Test : Cold
Position : Scanivalve

Pressure Pa	Volts V
0	-0.07755
500	0.4329
1000	0.9358
1450	1.3796
2000	1.9342
2520	2.4559
3000	2.9375
3500	3.4352
4000	3.9386
4500	4.4321
5000	4.9261
4500	4.4306
4000	3.9345
3500	3.4337
3000	2.9392
2500	2.4374
2000	1.9375
1500	1.4382
1000	0.9351
500	0.4308
0	-0.0694

Regression Output:

Constant	67.35527
Std Err of Y Est	4.31062
R Squared	0.999993
No. of Observations	21
Degrees of Freedom	19

X Coefficient(s)	999.5387
Std Err of Coef.	0.618379



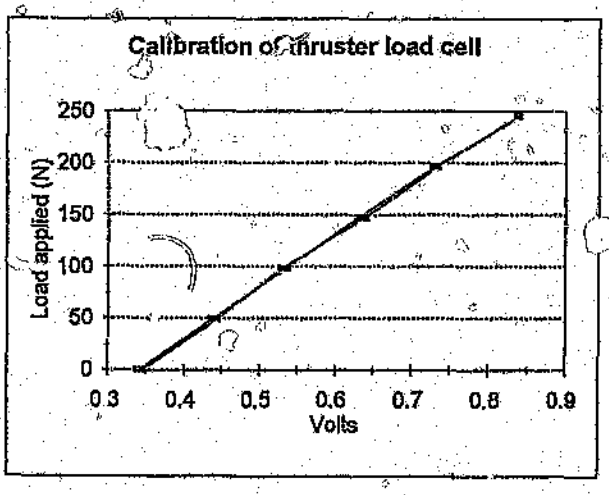
Calibration of thruster load cell
Test : Hot & Cold

Load Applied N	Volts V
0	0.3452
49.1	0.4437
98.1	0.5302
147.2	0.6392
196.2	0.7332
245.25	0.8382
196.2	0.7293
147.2	0.6303
98.1	0.5359
49.1	0.4377
0	0.3403

Regression Output:

Constant	-170.227
Std Err of Y Est	2.317009
R Squared	0.999287
No. of Observations	11
Degrees of Freedom	9

X Coefficient(s)	499.5727
Std Err of Coef.	4.447079



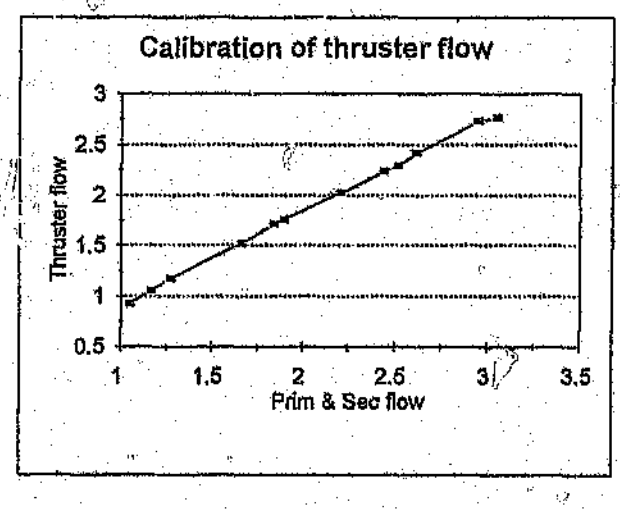
Calibration of thruster (with gauze in blower)

Sec	Prim	P + S	Thruster
2.603	0.453	3.056	2.764
2.497	0.456	2.953	2.726
2.153	0.463	2.616	2.415
2.057	0.461	2.518	2.29
1.985	0.462	2.447	2.235
1.746	0.467	2.213	2.025
1.427	0.471	1.898	1.755
1.373	0.472	1.845	1.713
1.189	0.477	1.666	1.521
0.797	0.482	1.279	1.172
0.686	0.485	1.171	1.058
0.565	0.488	1.053	0.9[illegible]4

Regression Output:

Constant	0.020291
Std Err of Y Est	0.023699
R Squared	0.998904
No. of Observations	12
Degrees of Freedom	10

X Coefficient(s)	1.08281
Std Err of Coef.	0.011343



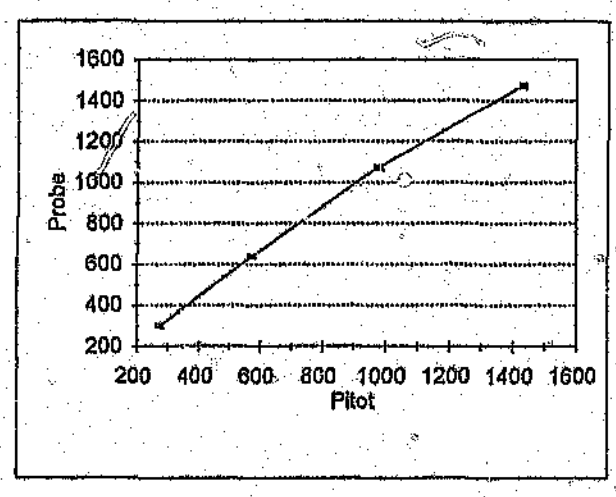
Calibration of static probe in thruster

Pitot	Probe
1430.667	1474.333
977.8333	1073.6
573.3333	638.1667
274.1667	299

Regression Output:

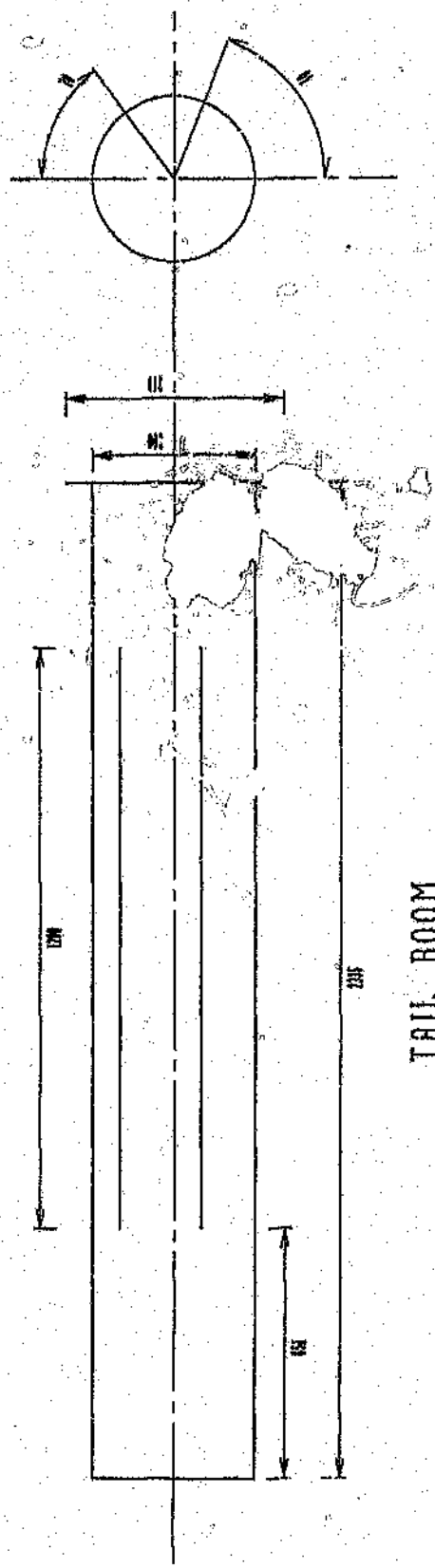
Constant	42.62403
Std Err of Y Est	35.52796
R Squared	0.99679
No. of Observations	4
Degrees of Freedom	2

X Coefficient(s)	1.017968
Std Err of Coef.	0.040849

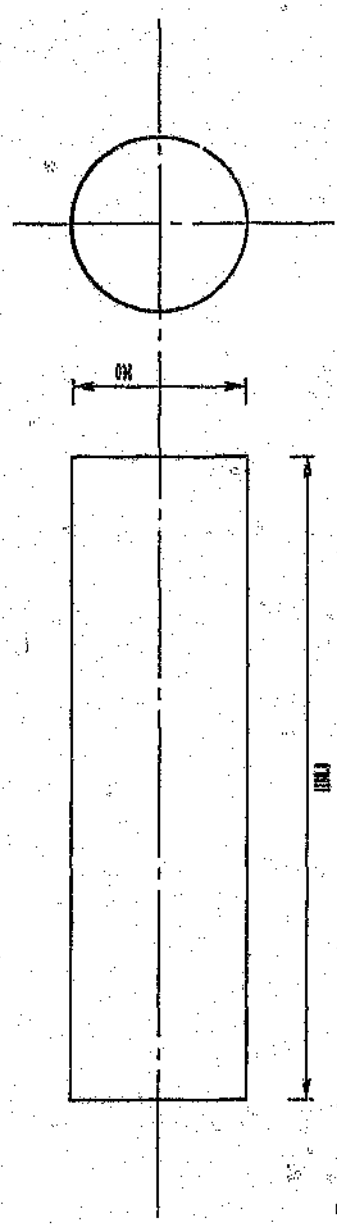


Appendix B

Drawings of Model

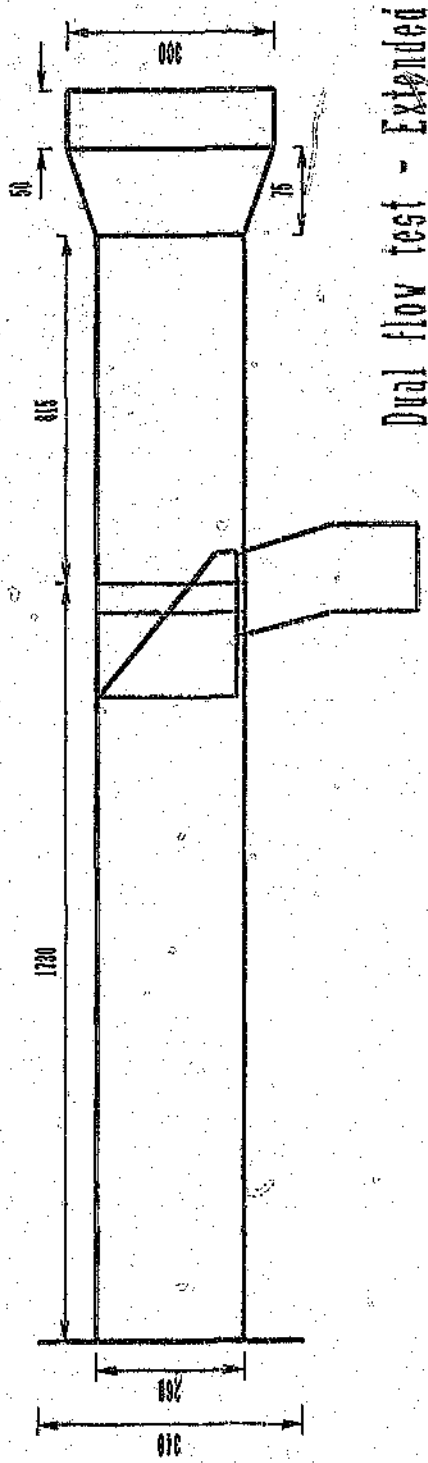


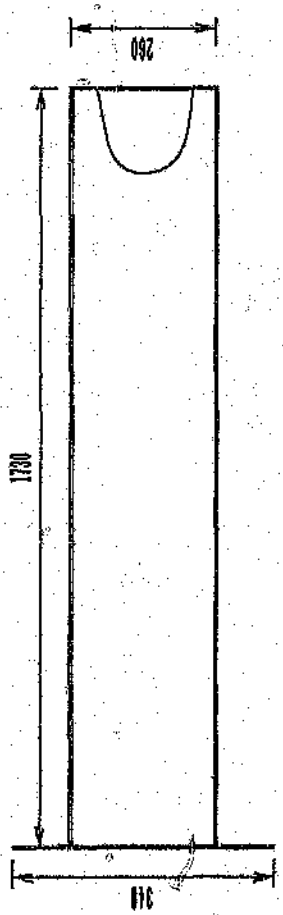
TAIL BOOM



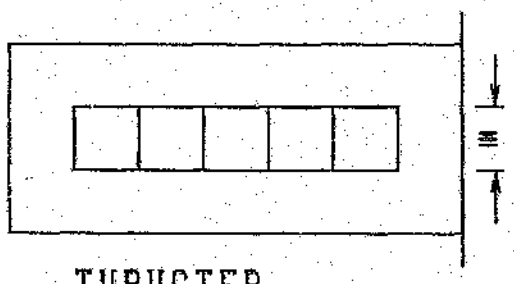
MIXING PIPE

Dual flow test - Extended inner pipe



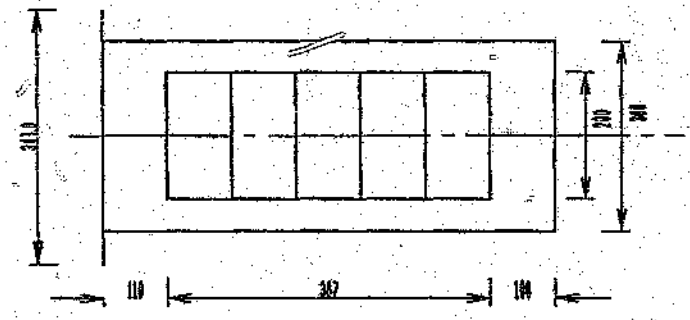




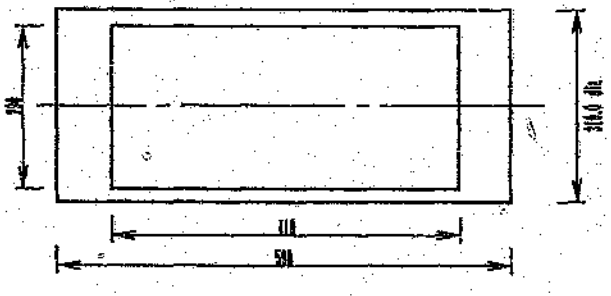


THRUSTER

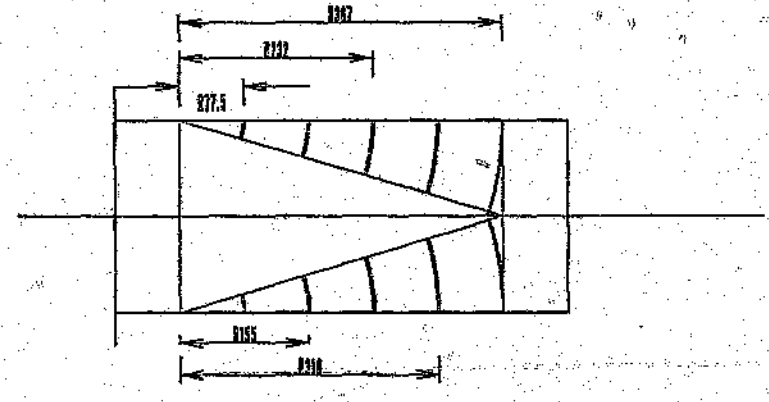
Small Outlet



THRUSTER LARGE OUTLET



CAN



THRUSTER BLADES

Appendix C

Tables of Results

Table C1: Results of hot tests: 4 fans running

Test - Hot - 4 fans		Point 1	Point 2	Point 3
Parameter	Position			
Thrust (N)		99.702	107.109	131.297
Flows (kg/s)	Primary	0.240	0.358	0.812
	Secondary	2.151	2.068	1.923
	Thruster	2.156	2.223	2.399
	CC-slots	0.235	0.203	0.338
Temperatures (°C)	Primary flow	16.864	16.841	16.035
	Burner	449.431	453.958	461.648
	Ambient	23.279	23.258	23.418
	Nozzle	415.494	418.005	416.404
	Thruster	128.083	132.573	155.457
	CC-slots	31.773	31.824	36.722
	Secondary flow	32.633	33.215	34.479
Pressure-static (Pa)	Sec flow on nozzle	1548	1591	1683
	Thruster	871	912	1259
	Prim flow in nozzle	1005	1048	1401
	Atmospheric	86905	86905	86905
Pressure total (Pa)	Thruster	1372	1555	2085
	Sec flow	1743	1779	1859
Density (kg/m^3)	Thruster	0.793	0.785	0.746
	Secondary flow	1.049	1.047	1.044
	Primary flow	0.509	0.536	0.623
Cp	Secondary flow	1.038	1.038	1.038
	Primary flow	1.110	1.110	1.110
	Thruster	1.050	1.060	1.060
APt		106.193	120.357	161.379
Power (W)	Thruster	3730.285	4405.525	6708.850
	Fan	3575.495	3513.490	3424.619
T^3/2/(A*rhoT)^0.5		4018.546	4498.518	6262.865
Velocity (m/s)	Secondary flow	39.905	38.893	33.203
	Primary flow	18.823	26.799	52.379
	Thruster	38.464	40.081	45.521
Ratios	Mass flow (Ge/Ga)	0.125	0.192	0.512
	Velocity (Ve/Va)	0.472	0.689	1.578
Kp	Thruster	0.928	0.979	1.071
	Fan	0.890	0.781	0.547
Kt	Thruster	0.939	0.890	0.814
Static pressure change	Engine exhaust g(Ge/Ga)	-0.601	-0.805	7.437
(Pa)	Fan air f(Ge/Ga)	-3.346	3.804	-0.079
Temperature Calc (°C)	Thruster	75.255	95.193	163.754

Constants	
Thruster Area (m^2) =	0.0774
Outer Diameter (m) =	0.3
Ab (m^2) =	0.07068583470577
Ae (m^2) =	0.0249

Table C2: Results of hot tests: 3 fans running

Test - Hot - 3 fans		Point 1	Point 2	Point 3	Point 4
Parameter	Position				
Thrust (N)		58.297	62.112	82.903	114.623
Flows (kg/s)	Primary	0.240	0.358	0.745	1.021
	Secondary	1.488	1.421	1.358	1.267
	Thruster	1.626	1.666	1.854	2.133
	CC-slots	0.102	0.113	0.249	0.155
Temperatures (°C)	Primary flow	15.962	13.960	12.996	12.536
	Burner	453.212	456.917	456.843	461.237
	Ambient	23.295	23.299	23.274	23.234
	Nozzle	418.806	420.474	413.858	408.365
	Thruster	137.396	143.882	177.629	198.634
	CC-slots	36.382	38.975	45.644	48.891
	Secondary flow	32.241	32.724	34.416	35.534
Pressure-static (Pa)	Sec flow on nozzle	957	945	976	1023
	Thruster	500	588	827	1017
	Prim flow in nozzle	712	760	924	1029
	Atmospheric	86905	869056	86905	86905
Pressure total (Pa)	Thruster	929	1029	1409	1868
	Sec flow	1093	1076	1102	1141
Density (kg/m^3)	Thruster	0.772	0.760	0.705	0.675
	Secondary flow	1.043	1.041	1.036	1.033
	Primary flow	0.506	0.532	0.612	0.745
Cp	Secondary flow	1.038	1.038	1.038	1.038
	Primary flow	1.111	1.111	1.110	1.108
	Thruster	1.060	1.060	1.060	1.070
APt		71.905	79.645	109.057	144.583
Power (W)	Thruster	1957.847	2254.916	3703.697	5900.295
	Fan	1559.459	1468.600	1444.848	1400.062
T^3/2/(A*rhoT)^0.5		1821.322	2017.749	3230.511	5367.171
Velocity (m/s)	Secondary flow	29.031	27.447	23.389	23.530
	Primary flow	19.039	27.007	48.906	55.012
	Thruster	29.815	31.001	37.187	44.685
Ratios	Mass flow (Ge/Ga)	0.173	0.274	0.672	0.918
	Velocity (Ve/Va)	0.656	0.984	2.091	2.338
Kp	Thruster	1.075	1.118	1.146	1.099
	Fan	0.856	0.728	0.447	0.261
Kt	Thruster	0.811	0.780	0.760	0.793
Static pressure change	Engine exhaust g(Ge/Ga)	-0.705	-1.597	2.025	1.785
(Pa)	Fan air f(Ge/Ga)	5.845	0.647	-0.275	-0.357
Temperature Calc (°C)	Thruster	89.289	116.029	186.874	213.960

Constants	
Thruster Area (m^2) =	0.0774
Outer Diameter (m) =	0.3
Ab (m^2) =	0.07068583470577
Ae (m^2) =	0.0249

Table C3: Results of hot tests: 2 fans running

Test - Hot - 2fans		Point 1	Point 2	Point 3	Point 4
Parameter	Position				
Thrust (N)		24.406	36.495	59.646	84.177
Flows (kg/s)	Primary	0.238	0.425	0.814	1.032
	Secondary	0.928	0.887	0.869	0.898
	Thruster	1.034	1.220	1.509	1.762
	CC-slots	0.132	0.092	0.174	0.168
Temperatures (°C)	Primary flow	18.501	16.927	15.439	13.588
	Burner	447.895	459.621	460.586	465.093
	Ambient	22.994	23.043	23.234	23.334
	Nozzle	416.102	420.499	415.784	411.084
	Thruster	150.876	183.142	214.507	232.477
	CC-slots	45.528	41.040	53.833	54.347
	Secondary flow	28.266	30.728	32.430	32.999
Pressure-static (Pa)	Sec flow on nozzle	513	477	483	477
	Thruster	329	397	517	618
	Prim flow in nozzle	363	411	499	476
	Atmospheric	86905	86905	86905	86905
Pressure total (Pa)	Thruster	669	822	1297	1406
	Sec flow	597	558	563	560
Density (kg/m^3)	Thruster	0.746	0.692	0.650	0.627
	Secondary flow	1.051	1.042	1.037	1.035
	Primary flow	0.516	0.558	0.627	0.752
Cp	Secondary flow	1.037	1.038	1.038	1.038
	Primary flow	1.110	1.111	1.110	1.090
	Thruster	1.060	1.070	1.070	1.070
APt		51.781	[illegible]	100.388	108.824
Power (W)	Thruster	928.025	1443.864	3013.138	3948.931
	Fan	526.967	474.823	471.951	486.039
T^3/2/(A*rhoT)^0.5		501.886	951.671	2054.175	3504.815
Velocity (m/s)	Secondary flow	16.544	16.652	14.651	15.410
	Primary flow	18.528	30.601	52.167	55.105
	Thruster	19.625	24.885	32.866	39.734
Ratios	Mass flow (Ge/Ga)	0.299	0.535	1.171	1.414
	Velocity (Ve/Va)	1.120	1.838	3.561	3.576
Kp	Thruster	1.849	1.519	1.467	1.127
	Fan	1.050	0.499	0.230	0.139
Kt	Thruster	0.471	0.574	0.594	0.774
Static pressure change	Engine exhaust g(Ge/Ga)	-3.007	4.984	0.955	1.227
(Pa)	Fan air f(Ge/Ga)	0.419	-0.336	-0.381	-0.391
Temperature Calc (°C)	Thruster	117.505	166.535	239.166	254.444

Constants	
Thruster Area (m^2) =	0.0774
Outer Diameter (m) =	0.3
Ab (m^2) =	0.07068583470577
Ae (m^2) =	0.0249

Table C4: Results of cold tests : 4 fans running

Test - Cold - 4 fans		Point 1	Point 2	Point 3
Parameter	Position			
Thrust (N)		149.705	140.349	103.012
Flows (kg/s)	Primary	0.458	0.455	0.461
	Secondary	2.699	2.618	2.232
	Thruster	2.991	2.896	2.481
	CC-slots	0.166	0.177	0.212
Pressure-static (Pa)	Sec flow on nozzle	2797	2620	2084
	Thruster	1535	1472	1067
	Prim flow in nozzle	291	280	249
	Atmospheric	87230	87230	87230
Pressure total (Pa)	Thruster	2326	2220	1721
	Sec flow	3058	2873	2300
Density (kg/m^3)	Thruster	1.017	1.017	1.017
	Secondary flow	1.017	1.017	1.017
	Primary flow	1.017	1.017	1.017
APt		180.032	171.828	133.205
Power (W)	Thruster	6843.922	6324.620	4200.554
	Fan	8118.770	7398.696	5049.774
T^3/2/(A*rhoT)^0.5		6529.923	5927.426	3727.225
Velocity (m/s)	Secondary flow	57.986	56.246	47.953
	Primary flow	18.093	17.975	16.212
	Thruster	41.626	40.304	34.529
Ratios	Mass flow (Ge/Ga)	0.170	0.174	0.207
	Velocity (Ve/Va)	0.312	0.320	0.380
Kp	Thruster	1.048	1.067	1.127
	Fan	1.243	1.248	1.355
Kt	Thruster	0.832	0.817	0.773
Static pressure change	Engine exhaust g(Ge/Ga)	-0.671	-0.901	-0.934
(Pa)	Fan air f(Ge/Ga)	-0.762	-0.734	-0.904

Constants	
Thruster Area (m^2) =	0.0774
Outer Diameter (m) =	0.3
Ab (m^2) =	0.070685834705770
Ae (m^2) =	0.0249

Table C5: Results of cold tests : 3 fans running

Test - Cold - 3 fans		Point 1	Point 2	Point 3
Parameter	Position			
Thrust (N)		95.701	87.534	69.346
Flows (kg/s)	Primary	0.460	0.461	0.467
	Secondary	2.136	2.034	1.806
	Thruster	2.392	2.287	2.036
	CC-slots	0.204	0.208	0.237
Pressure-static (Pa)	Sec flow on nozzle	1551	1398	961
	Thruster	1182	1093	891
	Prim flow in nozzle	300	29[illegible]	248
	Atmospheric	87230	8723[illegible]	87230
Pressure total (Pa)	Thruster	1517	142[illegible]	1119
	Sec flow	1758	1595	1136
Density (kg/m^3)	Thruster	1.017	1.017	1.017
	Secondary flow	1.017	1.017	1.017
	Primary flow	1.017	1.017	1.017
APt		117.416	110.218	86.611
Power (W)	Thruster	3568.800	3203.874	2240.873
	Fan	3693.771	3191.255	2016.339
T^3/2/(A*rho*T)^0.5		3337.572	2919.561	2058.657
Velocity (m/s)	Secondary flow	45.890	43.699	38.800
	Primary flow	18.172	18.212	18.449
	Thruster	33.282	31.830	28.331
Ratios	Mass flow (Ge/Ga)	0.215	0.227	0.259
	Velocity (Ve/Va)	0.396	0.417	0.475
Kp	Thruster	1.069	1.097	1.089
	Fan	1.107	1.093	0.979
Kt	Thruster	0.815	0.794	0.801
Static pressure change (Pa)	Engine exhaust g(Ge/Ga)	-1.115	-1.155	-1.369
	Fan air f(Ge/Ga)	-0.364	-0.335	-0.098

Constants	
Thruster Area (m^2) =	0.0774
Outer Diameter (m) =	0.3
Ab (m^2) =	0.07068583470577
Ae (m^2) =	0.0249

Table C6: Results of cold tests : 2 fans running

Test - Cold - 2 fans		Point 1	Point 2	Point 3
Parameter	Position			
Thrust (N)		49.568	46.199	31.924
Flows (kg/s)	Primary	0.471	0.473	0.478
	Secondary	1.465	1.399	1.160
	Thruster	1.721	1.662	1.381
	CC-slots	0.215	0.210	0.257
Pressure-static (Pa)	Sec flow on nozzle	802	701	376
	Thruster	712	661	495
	Prim flow in nozzle	193	175	116
	Atmospheric	87230	87230	87230
Pressure total (Pa)	Thruster	897	832	609
	Sec flow	944	836	488
Density (kg/m^3)	Thruster	1.017	1.017	1.017
	Secondary flow	1.017	1.017	1.017
	Primary flow	1.017	1.017	1.017
APt		69.428	64.397	47.137
Power (W)	Thruster	1518.688	1359.935	827.470
	Fan	1360.378	1150.486	756.837
T^3/2/(A*rhoT)^0.5		1244.088	1119.459	643.024
Velocity (m/s)	Secondary flow	31.474	30.056	24.922
	Primary flow	18.607	18.686	18.883
	Thruster	23.952	23.124	19.222
Ratios	Mass flow (Ge/Ga)	0.322	0.338	0.412
	Velocity (Ve/Va)	0.591	0.622	0.758
Kp	Thruster	1.221	1.215	1.287
	Fan	1.093	1.028	0.866
Kt	Thruster	0.714	0.717	0.677
Static pressure change (Pa)	Engine exhaust g(Ge/Ga)	-2.242	-2.571	-28.852
	Fan air f(Ge/Ga)	-0.212	-0.107	0.465

Constants	
Thruster Area (m^2) =	0.0774
Outer Diameter (m) =	0.3
Ab (m^2) =	0.07068583470577
Ae (m^2) =	0.0249

Table C7: Results of dual flow tests: At/Ab = 0.62

Thruster area = 0.032895 m^2
Area ratio At/Ab = 0.62

	Point 1	Point 2	Point 3	Point 4	Point 5	Point 6	Point7	Point 8
No. fans on:	4	4	3	3	2	2	1	1
% Valve closed	0	50	0	50	0	50	0	50
Fan flow (kg/s)	1.474	1.337	1.187	1.100	0.719	0.623	0.284	0.227
Blower flow (kg/s)	0.453	0.496	0.537	0.562	0.622	0.644	0.718	0.736
Load (N)	94.144	83.675	68.821	61.384	33.787	27.627	9.689	6.629
Air density (kg/m^3)	1.0503	1.0503	1.0503	1.0503	1.0503	1.0503	1.0503	1.0503
Inlet static (Pa)	3548.263	3252.379	2745.967	2546.175	1724.614	1561.484	752.197	610.233
Sec flow static-nozzle (Pa)	2416.423	2252.553	2047.453	1915.412	1484.295	1343.500	701.642	560.301
Prim flow-nozzle (Pa)	2240.692	2056.411	1932.003	1773.766	1365.190	1200.972	605.320	449.645
Thruster static (Pa)	2470.780	2269.336	2067.528	1910.667	1524.416	1392.041	1039.068	972.286
Ve (m/s)	17.329	18.978	20.551	21.495	23.773	24.641	27.471	28.160
Va (m/s)	26.428	23.981	21.289	19.734	12.894	11.173	5.095	4.063
Vf (m/s)	34.555	32.882	30.927	29.814	24.043	22.729	17.979	17.270
Pt thruster (Pa)	627.071	567.790	502.306	466.805	303.577	271.306	169.752	156.630
APt	48.535	43.947	38.878	36.131	23.497	20.999	13.139	12.123
T (N)	108.559	96.486	79.358	70.782	38.961	31.857	11.137	7.643
P (W)	2287.108	1970.576	1639.700	1468.977	770.399	650.879	322.131	285.511
T^3/2/(pA)^0.5	3979.026	3334.092	2486.946	2094.903	855.495	632.527	130.753	74.339
Kp fan	0.259	0.231	0.216	0.205	0.140	0.123	0.056	0.050
Ve/Va	0.656	0.791	0.965	1.089	1.844	2.205	5.391	6.930
f(Ve/Va)	4.140	3.699	2.567	2.423	0.926	0.824	-1.838	-2.447
g(Ve/Va)	-0.490	-0.562	-0.483	-0.611	-23.467	4.019	1.915	2.012

Table C8: Results of dual flow tests: At/Ab= 1.02

Thruster area = 0.05418 m^2
Area ratio = 1.02

	Point 1	Point 2	Point 3	Point 4	Point 5	Point 6	Point7	Point 8
No. fans on:	4	4	3	3	2	2	1	1
% Valve closed	0	50	0	50	0	50	0	50
Fan flow (kg/s)	2.052	1.849	1.683	1.537	1.195	1.039	0.642	0.520
Blower flow (kg/s)	0.698	0.709	0.722	0.732	0.742	0.754	0.765	0.785
Load (N)	129.730	109.450	91.504	76.926	53.351	40.884	17.076	10.244
Air density (kg/m^3)	1.0503	1.0593	1.0503	1.0503	1.0503	1.0603	1.0503	1.0503
Inlet static (Pa)	3425.000	3009.852	2430.975	2157.787	1462.067	1233.750	624.348	413.529
Sec flow static-nozzle (Pa)	1169.504	1017.524	953.514	874.527	702.533	607.964	432.056	251.273
Prim flow-nozzle (Pa)	710.977	601.601	662.401	681.893	448.071	364.801	250.660	60.817
Thruster static (Pa)	1422.184	1260.000	1109.782	1006.509	816.343	701.460	589.062	509.299
Ve (m/s)	26.705	27.116	27.591	27.972	28.376	28.844	29.265	30.025
Va (m/s)	36.791	33.158	30.184	27.566	21.429	18.633	11.520	9.324
Vf (m/s)	49.315	45.875	43.124	40.685	34.737	32.160	25.245	23.406
Pt thruster (Pa)	1277.156	1105.188	976.624	869.248	633.678	543.157	334.689	287.688
APt	98.852	85.542	75.591	67.280	49.047	42.040	25.905	22.267
T (N)	149.593	126.208	105.514	88.704	61.619	47.144	19.691	11.813
P (W)	6647.794	5351.386	4446.318	3732.736	2323.352	1843.742	891.814	710.713
T^3/2/(pA)^0.5	6436.477	4987.824	3812.792	2938.952	1697.451	1138.730	307.376	142.823
Kp fan	0.431	0.408	0.402	0.397	0.323	0.317	0.277	0.317
Ve/Va	0.726	0.818	0.914	1.015	1.324	1.548	2.540	3.220
f(Ve/Va)	3.537	3.298	2.652	2.448	1.645	1.475	0.133	-0.369
g(Ve/Va)	-0.788	-0.916	-0.793	-0.926	-1.747	-3.169	2.941	2.366

Table C9: Results of Dual flow tests: At/Ab = 1.22

Thruster area = 0.064629 m^2
Area ratio At/Ab= 1.22

	Point 1	Point 2	Point 3	Point 4	Point 5	Point 6	Point7	Point 8
No. fans on:	4	4	3	3	2	2	1	1
% Valve closed	0	50	0	50	0	50	0	50
Fan flow (kg/s)	2.2475	2.02	1.86	1.66	1.35	1.195	0.77	0.61
Blower flow (kg/s)	0.76725	0.768	0.77	0.778	0.774	0.7805	0.777	0.795
Load (N)	138.5908	112.7573	98.1645	78.517	59.49825	47.6865	22.66125	13.54375
Air density (kg/m^3)	1.0503	1.0503	1.0503	1.0503	1.0503	1.0503	1.0503	1.0503
Inlet static (Pa)	3305.699	2780.03	2306.594	1976.121		1150.671	562.074	332.604
Sec flow static-nozzle (Pa)	579.344	542.907	490.181	437.798	403.67	316.628	275.642	109.745
Prim flow-nozzle (Pa)	16.612	-32.824	113.23	89.905	71.01	630.696	50.686	-108.952
Thruster static (Pa)	912.552	794.251	700.491	613.939	517.96	441.278	408.937	320.226
Ve (m/s)	29.338	29.366	29.443	29.749	29.596	29.844	29.710	30.399
Va (m/s)	40.304	36.224	33.355	29.769	24.209	21.430	13.808	10.939
Vf (m/s)	54.063	49.997	47.163	43.720	38.089	35.426	27.742	26.196
Pt thruster (Pa)	1534.921	1312.711	1168.140	1003.809	761.890	659.079	404.170	333.377
APt	116.803	101.604	90.414	77.695	58.970	51.013	31.283	25.803
T (N)	159.810	130.022	113.194	90.539	68.608	54.988	26.131	15.617
P (W)	8758.730	6927.325	5815.064	4632.211	3063.027	2464.441	1183.473	886.577
T^3/2/(pA)^0.5	7107.011	5215.574	4236.596	3030.616	1999.133	1434.427	469.906	217.117
Kp fan	0.514	0.508	0.488	0.485	0.396	0.383	0.312	0.336
Ve/Va	0.728	0.811	0.883	0.999	1.222	1.393	2.152	2.779
f(Ve/Va)	3.510	3.184	2.751	2.530	-1.141	1.697	0.504	0.046
g(Ve/Va)	-0.827	-0.962	-0.824	-0.972	-1.480	0.990	6.033	2.825

Table C10: Results of dual flow tests: At/Ab = 1.48

Thruster area = 0.078561 m^2
Area ratio = 1.48

	Point 1	Point 2	Point 3	Point 4	Point 5	Point 6	Point7	Point 8
No. fans on:	4	4	3	3	2	2	1	1
% Valve closed	0	50	0	50	0	50	0	50
Fan flow (kg/s)	2.409	2.226	2.001	1.843	1.477	1.310	0.902	0.696
Blower flow (kg/s)	0.840	0.833	0.831	0.829	0.821	0.823	0.811	0.819
Load (N)	138.666	116.817	97.469	80.450	57.339	44.890	20.584	8.697
Air density (kg/m^3)	1.0503	1.0503	1.0503	1.0503	1.0503	1.0503	1.0503	1.0503
Inlet static (Pa)	3248.028	2778.661	2236.324	1938.705	1288.277	1070.022	500.012	284.228
Sec flow static-nozzle (Pa)	39.077	72.359	74.822	92.278	84.081	53.432	82.067	-2.712
Prim flow-nozzle (Pa)	-633.789	-591.560	-361.203	-319.604	-270.692	-278.118	-174.330	-255.261
Thruster static (Pa)	477.947	432.520	366.511	331.707	277.625	220.171	228.420	170.359
Ve (m/s)	32.114	31.863	31.760	31.689	31.398	31.467	31.004	31.311
Va (m/s)	43.265	39 917	35.889	33.044	26.486	23.489	16.177	12.487
Vf (m/s)	58.266	54.860	50.784	47.905	41.211	38.247	30.717	27.171
Pt thruster (Pa)	1702.845	1580.508	1354.367	1205.185	891.890	768.210	495.507	387.711
APt	137.992	122.331	104.828	93.281	69.032	59.459	38.352	30.009
T (N)	159.885	134.703	112.393	92.768	66.118	51.763	23.735	10.029
P (W)	**********	9151.810	7259.662	6093.865	3879.531	3101.218	1606.520	1111.922
T^3/2/(pA)^0.5	7112.013	5499.765	4191.658	3143.242	1691.284	1310.098	406.788	111.729
Kp fan	0.632	0.645	0.615	0.640	0.548	0.552	0.580	0.972
Ve/Va	0.743	0.798	0.885	0.959	1.185	1.340	1.917	2.508
f(Ve/Va)	3.452	3.154	2.758	2.544	1.931	1.776	0.758	0.372
g(Ve/Va)	-0.895	-0.978	-0.882	-0.961	-1.466	-2.007	43.398	3.347

Table C11 : Results of entrainment measurements

Blower Flowrate (m^3/s)	Entrainment Ratio (Ga/Ge)
1.296	0.515
0.903	0.510
0.692	0.498
0.553	0.509

Author: Bouwer Pieter.
Name of thesis: Experimental investigation of combined infra-red suppression and tail rotor elimination helicopter anti-torque system.

PUBLISHER:
University of the Witwatersrand, Johannesburg
©2015

LEGALNOTICES:

Copyright Notice: All materials on the University of the Witwatersrand, Johannesburg Library website are protected by South African copyright law and may not be distributed, transmitted, displayed or otherwise published in any format, without the prior written permission of the copyright owner.

Disclaimer and Terms of Use: Provided that you maintain all copyright and other notices contained therein, you may download material (one machine readable copy and one print copy per page)for your personal and/or educational non-commercial use only.

The University of the Witwatersrand, Johannesburg, is not responsible for any errors or omissions and excludes any and all liability for any errors in or omissions from the information on the Library website.